

A formulation of PANS capable of mimicking IDDES

Christophe Friess^{a,*}, Lars Davidson^b

^a M2P2 UMR 7340, Aix-Marseille Université, CNRS, Centrale Marseille, 13451 Marseille, France

^b Division of fluid dynamics, Department of Mechanics and Maritime Sciences, Chalmers University of Technology, SE-412 96 Gothenburg, Sweden

ARTICLE INFO

Keywords:

LES
PANS
IDDES
Channel flow
Hill flow
Hump flow

ABSTRACT

The partially averaged Navier–Stokes (PANS) model, proposed in [Girimaji \(2006\)](#), allows to simulate turbulent flows either in RANS, LES or DNS mode. The PANS model includes f_k which denotes the ratio of modeled to total kinetic energy. In RANS, $f_k = 1$ while in DNS it tends to zero. In the present study we propose an improved formulation for f_k based on the H -equivalence introduced by [Friess et al. \(2015\)](#). In this formulation the expression of f_k is derived to mimic Improved Delayed Detached Eddy Simulation (IDDES). This new formulation behaves in a very similar way as IDDES, even though the two formulations use different mechanisms to separate modeled and resolved scales. They show very similar performance in separated flows as well as in attached boundary layers. In particular, the novel formulation is able to (i) treat attached boundary layers as properly as IDDES, and (ii) “detect” laminar initial/boundary conditions, in which case it enforces RANS mode. Furthermore, it is found that the new formulation is numerically more stable than IDDES.

1. Introduction

The Partially Averaged Navier–Stokes (PANS) approach was originally proposed by [Girimaji \(2006\)](#), based on the scale separation between resolved and unresolved parts of the turbulent fluid motion, making use of the parameter f_k , which represents the modeled-to-total turbulent kinetic energy ratio. The way of prescribing f_k has been subject of a huge research effort. Recently, [Klapwijk et al. \(2019\)](#) made a comparative review of different ways of prescribing f_k , distinguishing two categories: static and dynamic formulations. Almost simultaneously with PANS, Partially Integrated Transport Model (PITM, see e.g. [Chaouat and Schiestel, 2005](#); [Schiestel and Dejoan, 2005](#)), was derived from multiscale approaches in spectral space, but also using the modeled-to-total turbulent kinetic energy ratio f_k .

Detached Eddy Simulation was developed almost a decade earlier, based on rather empirical fundaments, by [Spalart et al. \(1997\)](#). Their approach turned out to be very efficient in predicting unsteady features of flows out of equilibrium, but less so in flows involving thick boundary layers or shallow separations. A first improvement of DES was Delayed Detached Eddy Simulation (DDES) ([Spalart et al., 2006](#)), able to overcome the aforementioned issues. More recently, the DES community formulated Improved Delayed Detached Eddy Simulation (IDDES) ([Shur et al., 2008](#)), designed to act as a proper (i) wall-modeling approach for LES and (ii) RANS model when no turbulent content is provided in

initial/boundary conditions.

[Friess et al. \(2015\)](#) established an equivalence criterion between DES and other seamless hybrid RANS/LES approaches like PANS and PITM and formulated a postulate of equivalence: “Two hybrid approaches based on the same closure, but using a different method of control of the energy partition, yield similar low-order statistics of the resolved velocity fields provided that they yield the same level of subfilter energy.”. A by-product of that work is a new hybrid method, taking the shape of a DES designed with the energy ratio f_k instead of the explicit grid step Δ . Later, [Davidson and Friess \(2019\)](#) used this result the other way around, proposing a way to prescribe f_k in PANS (as well as in PITM) derived from the so-called “DES97” methodology. The model is denoted D-PANS. This formulation showed several interesting features (behaviour very similar to that of actual DES, self-adaptivity, better performance than PANS with fixed f_k ...) The present project aims at developing an improved formulation for f_k , gathering the interesting features of IDDES enumerated above, and the strong theoretical background of PANS.

The paper is organized as follows. First, the rationale of PANS, IDDES and the derivation of their equivalence criterion, is presented in Section 2. This derivation leads to a new approach, that will be called IDD-PANS. The solver used for the computations is presented in Section 3. In Section 4, IDDES and IDD-PANS, along with the D-PANS approach, are compared in three different flows (channel flow, hump flow and hill flow). Some conclusions are drawn in the final section.

* Corresponding author.

E-mail addresses: christophe.friess@univ-amu.fr (C. Friess), lada@chalmers.se (L. Davidson).

2. Rationale

In this section, the PANS and IDDES models are presented. They use different cutoff functions, to perform the separation between resolved and unresolved scales. Note that the unresolved scales correspond to the subgrid scales in LES mode, and to the modeled scales in RANS.

- PANS controls the destruction of unresolved dissipation, through the adaptive coefficient C_{e2}^* . Moreover, in PANS, diffusion coefficients are also tuned according to the cutoff. The idea is to damp modeled turbulent kinetic energy as the resolution gets finer.
- Though using the same idea of damping the modeled turbulent kinetic energy as above, DES and IDDES act in a more direct way. The sink term entering the unresolved turbulent kinetic energy equation is multiplied by an adaptive coefficient ψ .

Details are given below.

2.1. The PANS model

The low-Reynolds number Partially-Averaged Navier–Stokes (LRN PANS, see Ma et al. (2011)) uses the AKN $k-\varepsilon$ turbulence model (Abe et al., 1994) as parent RANS and reads

$$\begin{aligned} \frac{Dk_u}{Dt} &= \frac{\partial}{\partial x_j} \left[\left(\nu + \frac{\nu_{tu}}{\sigma_{ku}} \right) \frac{\partial k_u}{\partial x_j} \right] + P_{ku} - \varepsilon_u \frac{D\varepsilon_u}{Dt} \\ &= \frac{\partial}{\partial x_j} \left[\left(\nu + \frac{\nu_{tu}}{\sigma_{eu}} \right) \frac{\partial \varepsilon_u}{\partial x_j} \right] + C_{e1} P_{ku} \frac{\varepsilon_u}{k_u} - C_{e2}^* \frac{\varepsilon_u^2}{k_u} \nu_{tu} = C_{\mu} f_{\mu} \frac{k_u^2}{\varepsilon_u}, P_{ku} \\ &= 2\nu_{tu} \bar{s}_{ij} \bar{s}_{ij}, \bar{s}_{ij} = \frac{1}{2} \left(\frac{\partial \bar{v}_i}{\partial x_j} + \frac{\partial \bar{v}_j}{\partial x_i} \right) C_{e2}^* = C_{e1} + \frac{f_k}{f_\varepsilon} \left(C_{e2} f_2 - C_{e1} \right), \sigma_{ku} \\ &\equiv \sigma_k \frac{f_k^2}{f_\varepsilon}, \sigma_{eu} \equiv \sigma_\varepsilon \frac{f_\varepsilon^2}{f_\varepsilon} \sigma_k = 1.4, \sigma_\varepsilon = 1.4, C_{e1} = 1.5, C_{e2} = 1.9, C_\mu = 0.09 \end{aligned} \quad (1)$$

where $D/Dt = \partial/\partial t + \bar{v}_j \partial/\partial x_j$ denotes the material derivative. The damping functions are given by

$$\begin{aligned} f_2 &= \left[1 - \exp\left(-\frac{y^*}{3.1}\right) \right]^2 \left\{ 1 - 0.3 \exp\left[-\left(\frac{R_{tu}}{6.5}\right)^2\right] \right\} \\ f_\mu &= \left[1 - \exp\left(-\frac{y^*}{14}\right) \right]^2 \left\{ 1 + \frac{5}{R_{tu}^{3/4}} \exp\left[-\left(\frac{R_{tu}}{200}\right)^2\right] \right\} \\ R_{tu} &= \frac{k_u^2}{\nu \varepsilon_u}, \quad y^* = \frac{U_\varepsilon y}{\nu}, \quad U_\varepsilon = (\varepsilon_u \nu)^{1/4} \end{aligned} \quad (2)$$

The subscript u refers to the unresolved motion. The functions f_k and f_ε denote the ratio of modeled to total kinetic energy and modeled to total dissipation, respectively. For flows at high Reynolds numbers (as in the present work), the dissipation is modeled which means that $f_\varepsilon = 1$. In the PITM model, $\sigma_{ku} \equiv \sigma_k$ and $\sigma_{eu} \equiv \sigma_\varepsilon$. Note that, in PANS, C_{e2}^* is the control parameter for the resolution, with $\psi = 1$ (its RANS value).

2.2. The IDDES model

The aforementioned LRN model can be transposed to an IDDES form, also based on the AKN $k-\varepsilon$ turbulence model as parent RANS:

$$\begin{aligned} \frac{Dk_u}{Dt} &= \frac{\partial}{\partial x_j} \left[\left(\nu + \frac{\nu_{tu}}{\sigma_{ku}} \right) \frac{\partial k_u}{\partial x_j} \right] + P_{ku} - \psi \varepsilon_u \frac{D\varepsilon_u}{Dt} \\ &= \frac{\partial}{\partial x_j} \left[\left(\nu + \frac{\nu_{tu}}{\sigma_{eu}} \right) \frac{\partial \varepsilon_u}{\partial x_j} \right] + C_{e1} P_{ku} \frac{\varepsilon_u}{k_u} - C_{e2} f_2 \frac{\varepsilon_u^2}{k_u} \nu_{tu} = C_{\mu} f_{\mu} \frac{k_u^2}{\varepsilon_u}, P_{ku} \\ &= 2\nu_{tu} \bar{s}_{ij} \bar{s}_{ij}, \bar{s}_{ij} = \frac{1}{2} \left(\frac{\partial \bar{v}_i}{\partial x_j} + \frac{\partial \bar{v}_j}{\partial x_i} \right) \sigma_k = 1.4, \sigma_\varepsilon = 1.4, C_{e1} = 1.5, C_{e2} \\ &= 1.9, C_\mu = 0.09 \end{aligned} \quad (3)$$

The damping functions are the same as in the LRN PANS model (given by Eq. (2)).

Note that, in (ID)DES, ψ is the control parameter for the resolution, while C_{e2} is set to its RANS value. The function ψ may be more or less sophisticated. In all cases, we write ψ as:

$$\psi = \frac{l_u}{\tilde{l}}. \quad (4)$$

Let us define three length scales:

- l_u , the characteristic (local and instantaneous) length scale of the unresolved scales,
- l_c , the characteristic length scale of the cutoff,
- \tilde{l} , the reference length scale.

Those length scales read

$$l_u = \frac{k_u^{3/2}}{\varepsilon_u}, \quad (5)$$

and

$$l_c = C_{DES} \Delta. \quad (6)$$

The key difference between DES and IDDES lies in the prescription of \tilde{l} entering Eq. (4). In original DES, the reference length scale \tilde{l} simply reads:

$$\tilde{l} = \min(l_u; l_c). \quad (7)$$

In IDDES, it is more sophisticated. The grid step Δ is also chosen in a more complex way. These differences are discussed below.

2.2.1. Cut-off length scale

The cut-off length scales is defined as:

$$l_c = \Psi C_{DES} \Delta, \quad (8)$$

where Ψ is a low-Reynolds number correction (see Eq. 10), and Δ :

- the maximum grid step h_{max} in DES,
- a *corrected* grid step, designed to improve the WMLES (wall-modeled LES) capabilities of DES. It reads:

$$\Delta = \min\{\max[C_w d_w; C_w h_{max}; h_{wn}]; h_{max}\}, \quad (9)$$

where

- $C_w = 0.15$ is a constant, presumably independent of the turbulent closure,
- d_w is the distance to the closest wall,
- h_{wn} is the grid step in the wall normal direction.

The low-Reynolds correction Ψ (see e.g. Shur et al., 2008; Spalart

et al., 2006) depends on the turbulent closure, and is set so that at equilibrium (neither convection nor diffusion in the closure equations), the eddy viscosity obeys a Smagorinsky-like law, in LES mode. This correction is only needed for closure models using some low-Reynolds features, which is the case of the model used here, and summarized in Eq. (1), and Ψ reads:

$$\Psi = \min\left\{10; (f_2 f_\mu)^{-3/4}\right\} \quad (10)$$

where f_2 and f_μ are given by Eq. 2.1 and the limiting value of 10 is added to ensure reasonable behavior of Ψ in the “DNS limit”, i.e. $\nu_{tu} < \nu/100$, as prescribed in Spalart et al. (2006). Details on the calibration of Ψ are given in Appendix A.

2.2.2. Reference length scale

In contrast with its formulation given by Eq. (7) in DES, the reference length scale \tilde{l} is, in IDDES, a blending between l_u and l_c . It reads:

$$\tilde{l} = \tilde{f}_d(1 + f_e)l_u + (1 - \tilde{f}_d)l_c, \quad (11)$$

where l_u is defined by (5) and l_c by (8). The blending functions \tilde{f}_d and f_e read:

$$\tilde{f}_d = \max\{(1 - f_{dt}); f_B\}, \quad (12)$$

$$f_e = \max\{(f_{e1} - 1); 0\} \Psi f_{e2}, \quad (13)$$

where Ψ is given by Eq. (10) and the functions f_{dt} and f_B entering Eq. (12) are given by:

$$f_{dt} = 1 - \tanh[(8r_{dt})^3], \quad (14)$$

$$f_B = \min\{2\exp(-9\alpha^2); 1\}, \quad (15)$$

with

$$\alpha = 0.25 - d_w/h_{max}. \quad (16)$$

The functions f_{e1} and f_{e2} in Eq. (13) read:

$$f_{e1} = \begin{cases} 2\exp(-11.09\alpha^2) & \text{if } \alpha \geq 0 \\ 2\exp(-9\alpha^2) & \text{if } \alpha < 0 \end{cases}, \quad (17)$$

and

$$f_{e2} = 1 - \max\{f_i; f_l\}, \quad (18)$$

where the functions f_i and f_l are given by:

$$f_i = \tanh[(c_i^2 r_{dt})^3], \quad (19)$$

$$f_l = \tanh[(c_l^2 r_{dl})^{10}]. \quad (20)$$

The constants c_t and c_l above, depend on the background RANS model. They were originally tuned in Shur et al. (2008) for the SA model, and later in Gritskevich et al. (2012) for the $k-\omega$ SST model. The chosen values are $c_t = 1.87$ and $c_l = 5$.

The quantities r_{dt} (also entering Eq. 14) and r_{dl} , are defined as follows:

$$r_{dt} = \frac{\nu_t}{\kappa^2 d_w^2 \max\{\mathcal{S}; 10^{-10}\}}, \quad (21)$$

$$r_{dl} = \frac{\nu}{\kappa^2 d_w^2 \max\{\mathcal{S}; 10^{-10}\}}, \quad (22)$$

where

$$\mathcal{S} = \sqrt{\sum_j \left(\frac{\partial u_i}{\partial x_j}\right)^2}. \quad (23)$$

In what follows, we derive a relationship between the cutoff control functions ψ of IDDES and f_k (or equivalently, C_{e2}^*) of PANS.

2.3. Equivalence between PANS and DES/IDDES

Friess et al. (2015) made a first attempt in bridging DES and PITM. They derived equivalence criteria in three major cases:

- homogeneous equilibrium layers,
- inhomogeneous flows,
- allowing filter-induced modifications of the unresolved dissipation rate (while the two previous cases assume that it is not affected by the energy partition).

In that aim, they considered infinitesimal perturbations in the equilibrium of the ensemble-averaged $k_u - \varepsilon_u$ system, when introducing $\delta\psi$ for DES and δC_{e2}^* for PITM, given that in RANS mode, $\psi = f_k = 1$ and $C_{e2}^* = C_{e2}$. Then, integrating the result between RANS and an arbitrary state, yields a relationship evaluating ψ for a given f_k .

More recently, Davidson and Friess (2019) used the aforementioned relationship in a reverse way, in order to obtain some new way to define the f_k factor for PANS, ψ being given by DES (see Eqs. (5)–(7) in the present paper). However, their work was a first attempt, as (i) they just considered the homogeneous equilibrium layer case in their derivation and (ii) they restricted their study to DES. In Davidson and Friess (2018), they showed that this method works pretty much like DES.

Now, in the present work, we consider inhomogeneous flows, which are more relevant in engineering. Let us define k_M and ε_M such as:

$$k_M = \langle k_u \rangle \quad (24)$$

$$\varepsilon_M = \langle \varepsilon_u \rangle \quad (25)$$

where $\langle \cdot \rangle$ denotes the ensemble average. Along mean streamlines, k_M and ε_M are assumed to be in equilibrium, which yields, when describing both PANS and (ID)DES:

$$\frac{Dk_M}{Dt} = P^k + D^k - \psi \varepsilon_M = 0 \quad (26)$$

$$\frac{D\varepsilon_M}{Dt} = C_{e1} \frac{\varepsilon_M}{k_M} P^k + D^e - C_{e2}^* \frac{\varepsilon_M^2}{k_M} = 0 \quad (27)$$

where P^k denotes the production of k_M and D^k and D^e the diffusion terms of k_M and ε_M respectively.

In order to perform the perturbation analysis, some assumptions are needed. First, since in Section 2.1, we assumed that $f_e = 1$, it yields:

$$\delta \varepsilon_M = 0 \quad (28)$$

Following Friess et al. (2015), we add the heuristic assumption that the relative variation $\delta k_M/k_M$ does not vary in space, which allows to state:

$$\frac{\partial(k_M + \delta k_M)}{\partial x_j} = \left(1 + \frac{\delta k_M}{k_M}\right) \frac{\partial k_M}{\partial x_j} \quad (29)$$

$$\frac{\partial^2(k_M + \delta k_M)}{\partial x_j \partial x_j} = \left(1 + \frac{\delta k_M}{k_M}\right) \frac{\partial^2 k_M}{\partial x_j \partial x_j} \quad (30)$$

Furthermore, by definition,

$$f_k = k_M/k_{tot} \quad (31)$$

where k_{tot} is the total (resolved + modeled) turbulent kinetic energy.

2.3.1. PANS equations

For the PANS method ($\psi=1$), the equations for infinitesimal perturbations of Eqs. (26)–(27) are:

$$\delta P^k + \delta D^k = 0 \quad (32)$$

$$C_{e1} \frac{\varepsilon_M}{k_M} P^k \left(\frac{\delta P^k}{P^k} - \frac{\delta k_M}{k_M} \right) - C_{e2} \frac{\varepsilon_M^2}{k_M} \left(\frac{\delta C_{e2}^*}{C_{e2}^*} - \frac{\delta k_M}{k_M} \right) + \delta D^e = 0 \quad (33)$$

At sufficiently high Reynolds number, the diffusion terms D^k and D^e can be written:

$$D^k = \frac{\partial}{\partial x_j} \left[\frac{C}{\sigma_k f_k^2} \frac{k_M^2}{\varepsilon_M} \frac{\partial k_M}{\partial x_j} \right] \quad (34)$$

$$D^e = \frac{\partial}{\partial x_j} \left[\frac{C}{\sigma_e f_k^2} \frac{k_M^2}{\varepsilon_M} \frac{\partial \varepsilon_M}{\partial x_j} \right] \quad (35)$$

Using Eqs. (28)–(31) to differentiate Eqs. (34) and (35), it can be shown that:

$$\frac{\delta D^k}{D^k} = \frac{\delta k_M}{k_M} \quad (36)$$

$$\frac{\delta D^e}{D^e} = 0 \quad (37)$$

Thus, the following relation is obtained:

$$\delta C_{e2}^* = (C_{e2}^* - C_{e1}) \frac{\delta k_M}{k_M} \quad (38)$$

2.3.2. (ID)DES equations

The same procedure is done with the (ID)DES system ($C_{e2}^* = C_{e2}$). The equations for infinitesimal perturbations of Eqs (26)–(27) are:

$$\delta P^k + \delta D^k + \varepsilon_M \delta \psi = 0 \quad (39)$$

$$C_{e1} \frac{\varepsilon_M}{k_M} P^k \left(\frac{\delta P^k}{P^k} - \frac{\delta k_M}{k_M} \right) + C_{e2} \frac{\varepsilon_M^2}{k_M} \left(\frac{\delta k_M}{k_M} \right) + \delta D^e = 0 \quad (40)$$

At sufficiently high Reynolds number, the diffusion terms D^k and D^e can be written:

$$D^k = \frac{\partial}{\partial x_j} \left[\frac{C}{\sigma_k} \frac{k_M^2}{\varepsilon_M} \frac{\partial k_M}{\partial x_j} \right] \quad (41)$$

$$D^e = \frac{\partial}{\partial x_j} \left[\frac{C}{\sigma_e} \frac{k_M^2}{\varepsilon_M} \frac{\partial \varepsilon_M}{\partial x_j} \right] \quad (42)$$

Note that, contrary to PANS, there is no f_k correction in the diffusivity. Like for PANS above, we use Eqs. (28)–(31) to differentiate Eqs. (41) and (42). As a result, it can be shown that

$$\frac{\delta D^k}{D^k} = 3 \frac{\delta k_M}{k_M} \quad (43)$$

$$\frac{\delta D^e}{D^e} = 2 \frac{\delta k_M}{k_M} \quad (44)$$

As a result, the following relation is obtained:

$$\delta \psi = 3 \frac{(C_{e1}\psi - C_{e2})}{C_{e1}} \frac{\delta k_M}{k_M} \quad (45)$$

Now, equalizing $\delta k_M/k_M$ in Eqs. (38) and (45) and integrating the obtained relation between RANS ($C_{e2}^* = C_{e2}$ and $\psi = 1$) and an arbitrary state, yields:

$$\int_{C_{e2}}^{C_{e2}^*} \frac{x}{x - C_{e1}} = \int_1^\psi -\frac{C_{e1} dy}{3C_{e1}y - C_{e2}} \Rightarrow \ln \left(\frac{C_{e2}^* - 1}{C_{e2} - 1} \right) = \frac{1}{3} \ln \left(\frac{C_{e1}\psi - C_{e2}}{C_{e2} - C_{e1}} \right) \quad (46)$$

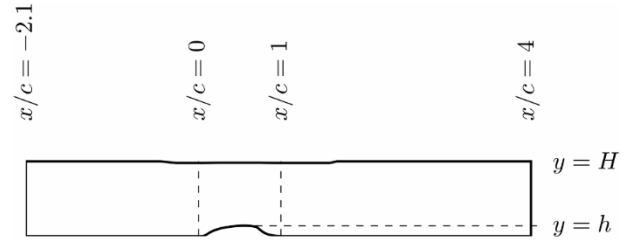


Fig. 1. The geometry of the hump.

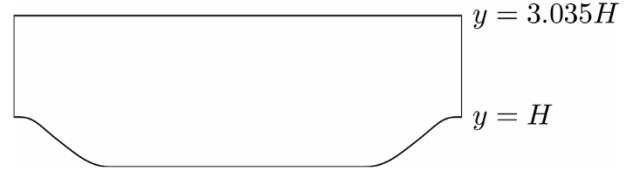


Fig. 2. The geometry of the hill.

As a consequence, when ensuring that $0 \leq f_k \leq 1$ we get

$$f_k = \min \left[1, \max \left(0, \left(\frac{C_{e2} - C_{e1}\psi}{C_{e2} - C_{e1}} \right)^{1/3} \right) \right] \quad (47)$$

It is worth mentioning that the relationship (47) was derived without assuming the way of defining ψ , i.e. regardless of whether ψ is defined in a DES or an IDDES way. However, since we aim at building a formulation of PANS that is equivalent to IDDES, we will consider the latter, (i.e. ψ is defined through Eqs. (4), (5), (8) and (11)).

3. Numerical solver

An incompressible, finite volume code is used (Davidson and Peng, 2003). The convective terms in the momentum equations are discretized using central differencing. Hybrid central/upwind is used for the k_u and ε_u equations. The Crank–Nicolson scheme is used for time discretization of all equations. The numerical procedure is based on an implicit, fractional step technique with a multigrid pressure Poisson solver (Emvin, 1997) and a non-staggered grid arrangement.

The filtered momentum equations with an added turbulent viscosity ν_{tu} to account for the effect of the unresolved scales on the resolved motion, read

$$\frac{\partial \bar{v}_i}{\partial t} + \frac{\partial \bar{v}_j \bar{v}_i}{\partial x_j} = \beta \delta_{1i} - \frac{1}{\rho} \frac{\partial \bar{p}}{\partial x_i} + \frac{\partial}{\partial x_j} \left((\nu + \nu_{tu}) \frac{\partial \bar{v}_i}{\partial x_j} \right) \quad (48)$$

where the first term on the right side is the driving pressure gradient in the streamwise direction, which is used in the fully-developed channel flow simulations and for the hill flow.

4. Results

In order to validate the IDDES capabilities of the approach developed in Section 2, denoted *IDD-PANS*, we will now perform a comparison of *IDD-PANS* with actual IDDES, using the same turbulent closure model (AKN). In IDDES, we compute ψ and its related coefficients using Eqs. (4)–(20), (22), (23). In *IDD-PANS*, the same ψ is used to prescribe $f_{k,tar}$ following Eq. (47). For the sake of performance comparison, results obtained with the *D-PANS* approach (also using the AKN closure model) are shown as well. It is worth recalling that there is a distinction to make between $f_{k,obs}$, the *observed* energy ratio defined as:

$$f_{k,obs} = \frac{k_M}{k_{tot}} \quad (49)$$

Table 1

Channel flow: mesh specifications.

Re_τ	$N_x = N_z$	N_y	Δx^+	Δz^+	Δy^+_{wall}	$\Delta y^+_{\text{center}}$
5200	32	96	520	260	0.5	677
2000	64	96	100	50	0.5	213

and $f_{k,tar}$, the *targeted* (or prescribed) energy ratio. In IDD-PANS $f_{k,tar} = f_k$ (computed in Eq. 47) is used, but there is usually a discrepancy between $f_{k,obs}$ and $f_{k,tar}$ (see e.g. Fadai-Ghotbi et al., 2010; Davidson and Friess, 2019 for discussion). Meanwhile, $f_{k,obs}$ can be obtained from post-processing, using its definition in Eq. (49).

The comparison is performed upon three test cases: the fully developed channel flow, the hump flow (see Fig. 1), and the hill flow (see Fig. 2).

The comparison is performed regarding various quantities:

- streamwise velocity,
- turbulent kinetic energy and shear stress: total moments, along with their repartition between modeled and resolved parts,
- $f_{k,obs}$ and $f_{k,tar}$,

along with case-specific quantities.

4.1. Channel flow

We consider a periodic channel flow at $Re_\tau = u_\tau \delta / \nu = 5200$ and 2000, where δ denotes half channel height and u_τ is the friction velocity. The streamwise, wall-normal and spanwise directions are denoted by x , y and z , respectively. The size of the domain is $x_{max} = 3.2$, $y_{max} = 2$ and $z_{max} = 1.6$. Two distinct meshes are used (see Table 1). The grid used for the $Re_\tau = 2000$ case is a fine, LES-like grid. Periodic boundary conditions are used in the x and z directions. Therefore, these two directions are considered statistically homogeneous. A precursor DES computation is used as initial condition. The driving pressure gradient (first term on the right hand side in Eq. 48) is used with $\beta = 1$. For the sake of numerical stability, a lower limit of 0.05 is used when computing $f_{k,tar}$ from Eq. (47). Two options on initial conditions, are considered:

- turbulent content (fluctuating),
- no turbulent content (steady),

4.1.1. Fluctuating case

Fig. 3(a) presents the mean velocity profile. As can be seen, IDD-PANS is able to match the IDDES profile, and thus performs better than D-PANS. Figs. 3(d) shows the ratio between production and dissipation rate of the total turbulent kinetic energy. A small logarithmic zone appears for all three approaches. This is consistent with the total turbulent kinetic energy k_{tot} (Fig. 3b) and shear stress $\tau_{12,tot}$ (Fig. 3c):

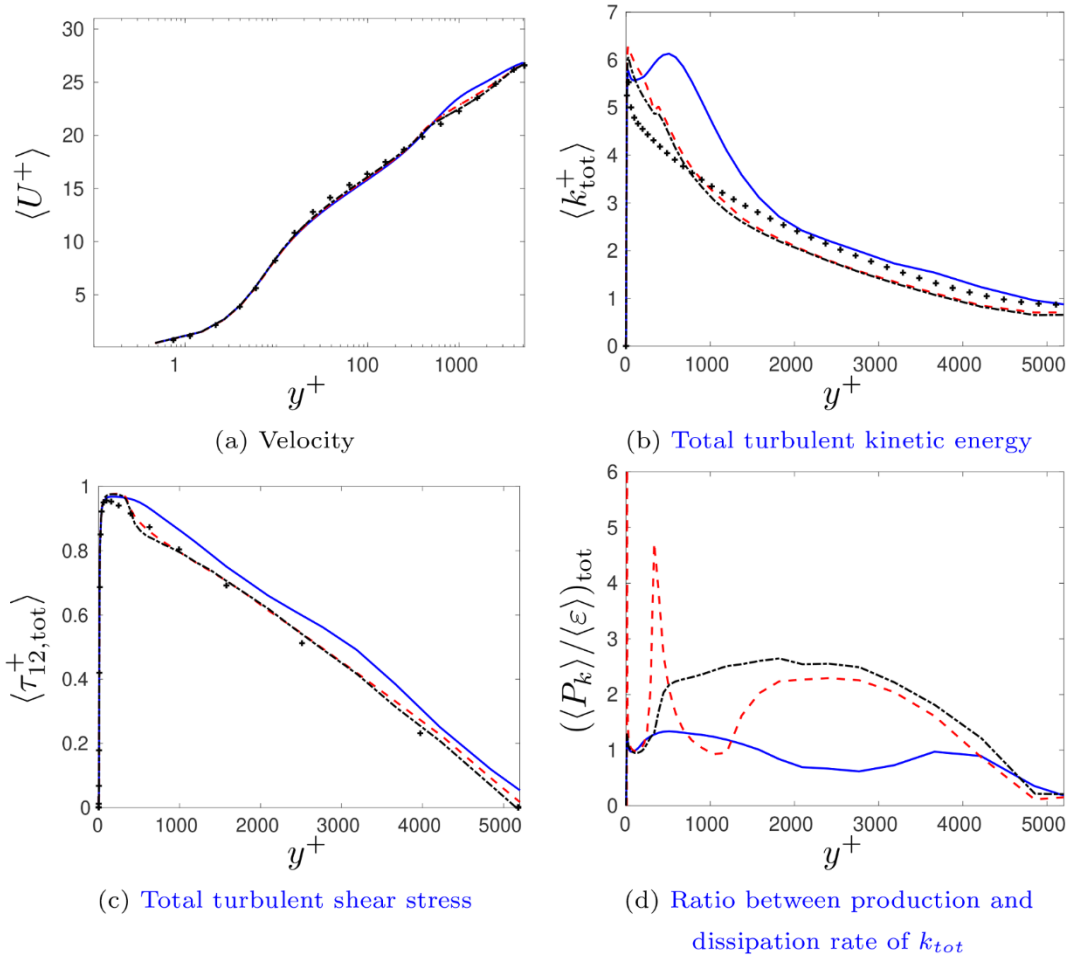


Fig. 3. Channel flow, $Re_\tau = 5200$. —: D-PANS; - - : IDD-PANS; - · - : IDDES; Markers: DNS (Lee and Moser, 2015).

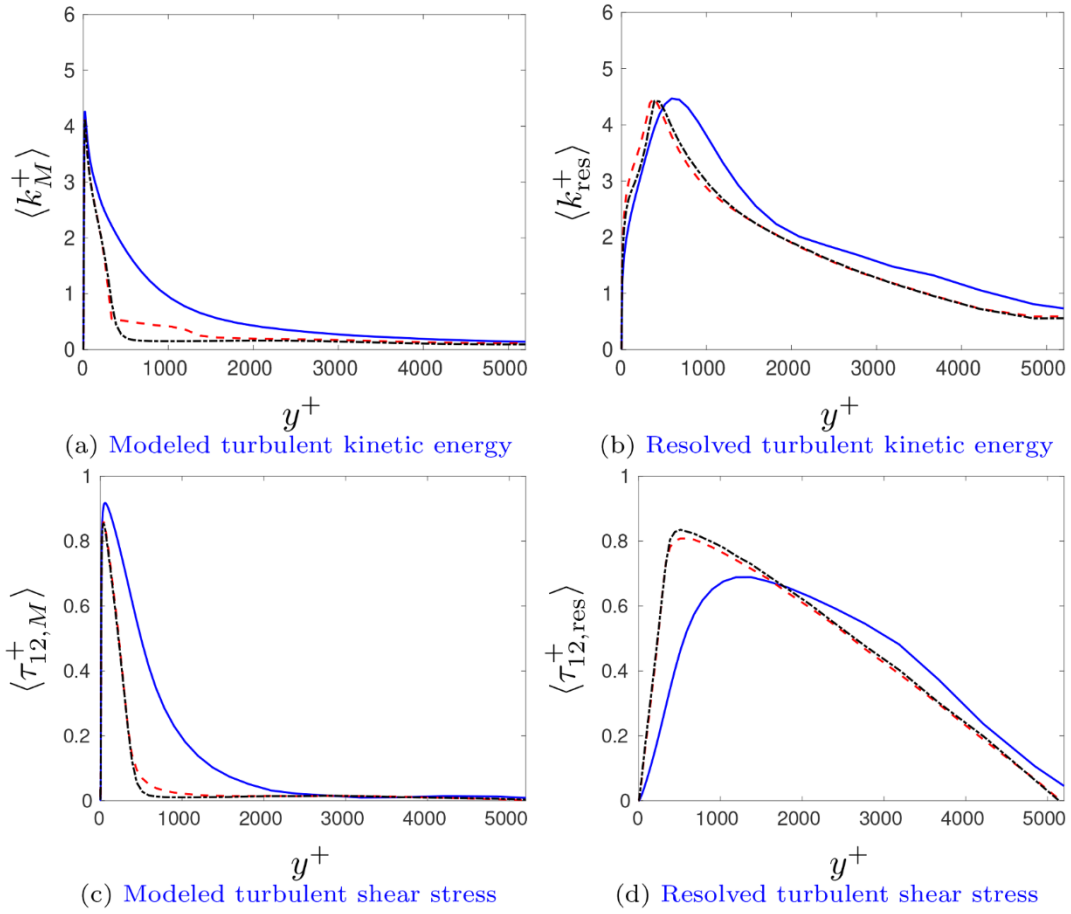


Fig. 4. Channel flow, $Re_\tau = 5200$. —: D-PANS; - - : IDD-PANS; - · - : IDDES; Markers: DNS (Lee and Moser, 2015).

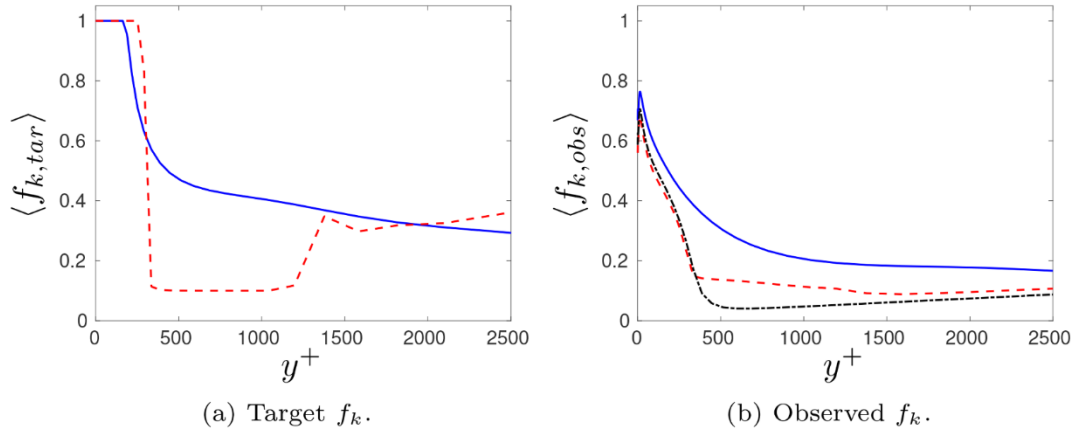


Fig. 5. Channel flow. f_k . $Re_\tau = 5200$. —: D-PANS; - - : IDD-PANS; - · - : IDDES.

both quantities exhibit peaks in this logarithmic region of the flow. However, it is worth noticing that the D-PANS k_{tot} profile exhibits a secondary peak. Accordingly, Figs. 4(a) and (b), showing respectively modeled and resolved k , show a stronger peak mismatch for D-PANS, than for the other two approaches. For their part, IDD-PANS and IDDES are in good agreement, even with the reference DNS.

Fig. 4(c) and (d) show respectively modeled and resolved parts of the turbulent shear stress τ_{12} . As about k , IDDES and IDD-PANS are in remarkable accordance, while D-PANS differs significantly from the two other approaches. This is consistent with the theoretical background leading to the equivalence criterion between IDD-PANS and IDDES developed in Section 2.3; in an equilibrium case like the channel flow,

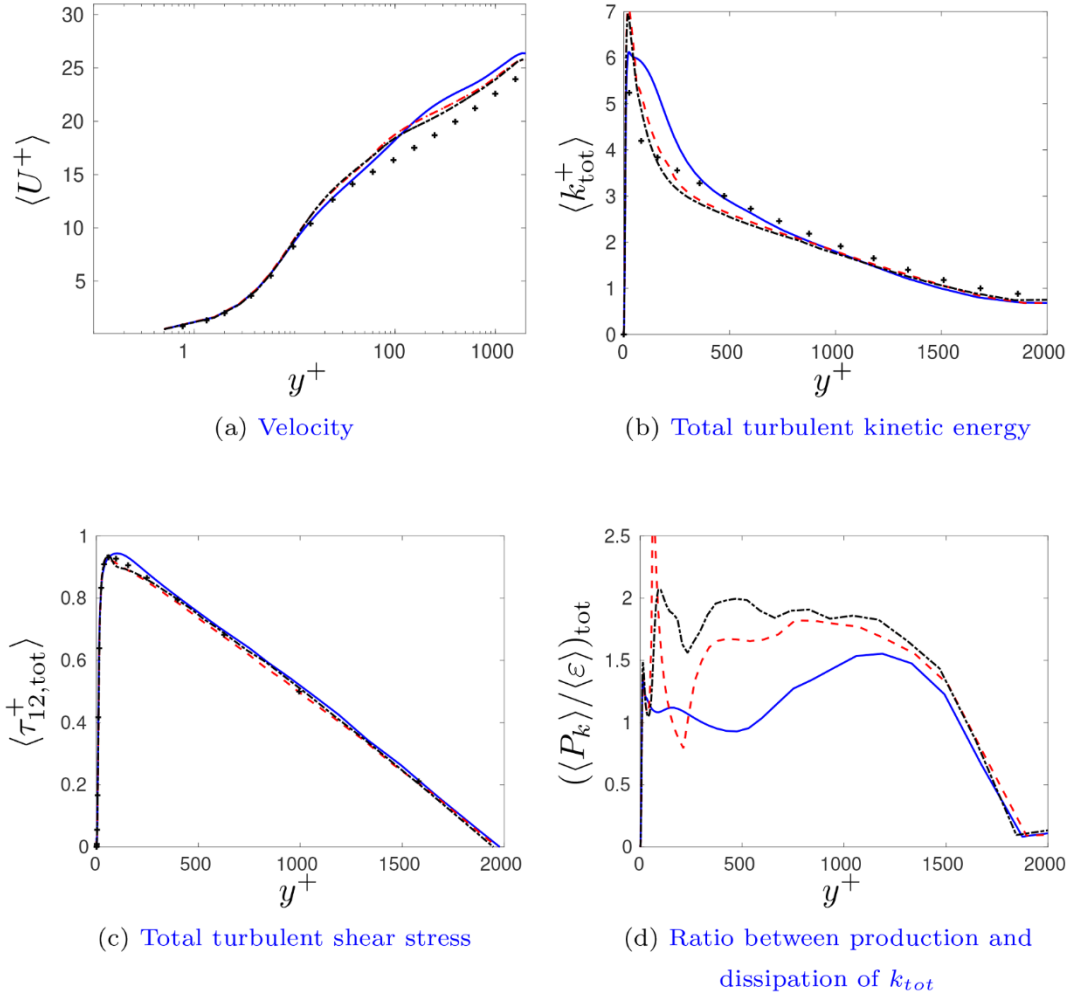


Fig. 6. Channel flow, $Re_\tau = 2000$. —: D-PANS; - - : IDD-PANS; - · - : IDDES; Markers: DNS (Lee and Moser, 2015).

IDD-PANS and IDDES must be equivalent. Eventually, it is also worth noticing that τ_{12} is overall more resolved than k . In other words, if we defined a τ_{12} -equivalent of f_k , called f_{12} , we would have $f_{12} < f_k$, especially toward the center of the channel.

Fig. 5(a) compares the target energy ratio $f_{k,tar}$ between D-PANS and IDD-PANS. Note that there is no $f_{k,tar}$ for the IDDES. The shape of the IDD-PANS profile is more complex than D-PANS. This can be explained by the fact that the construction of ψ_{IDDES} is more elaborate than ψ_{DES} , since IDDES is a further evolved version of DES. This complex shape of the IDD-PANS $f_{k,tar}$ profile generates strong wall-normal gradients of $f_{k,tar}$. Interestingly, the lowest plateau of IDD-PANS $f_{k,tar}$, near the wall, corresponds to the area where IDDES differs the most from IDD-PANS. Moreover, the aforementioned sharp wall-normal gradients of $f_{k,tar}$ seem diffused, such that the IDD-PANS $f_{k,obs}$ profile is more regular (see Fig. 5b). The latter shows the profiles of the observed energy ratio $f_{k,obs}$ between D-PANS, IDD-PANS and IDDES. As previously with total quantities, one can see that the IDD-PANS profile is very close to that of IDDES, illustrating again that IDD-PANS is able to mimic IDDES,

however only approximately.

Fig. 6(a) presents the mean velocity profile for the channel case at $Re_\tau = 2000$. As for the $Re_\tau = 5200$ case, IDD-PANS is able to match the IDDES profile, but performs only slightly better than D-PANS. However, IDDES and IDD-PANS do not match the DNS profile at all. This might be due to the fact that one assumption made earlier (all dissipation is contained in the modeled scales) is no longer valid in LES. Accordingly, Fig. 6(c) presents similar discrepancies between DNS and the three hybrid approaches, on the total turbulent shear stress profiles. Fig. 6(d) shows the ratio between production and dissipation rate of the total turbulent kinetic energy. A really tiny logarithmic zone appears for all three approaches. This is qualitatively consistent with the fact that Re_τ is lower than previously. Fig. 6(b) shows total turbulent kinetic energy profiles. Similarly as previously with the shear stress, IDDES and IDD-PANS are in good mutual accordance, but they differ from the reference DNS, but not as much as D-PANS, particularly in the near-wall region.

Fig. 7(c) and (d) show respectively modeled and resolved parts of the turbulent shear stress τ_{12} . Fig. 7(a) and (b) show the same repartition,

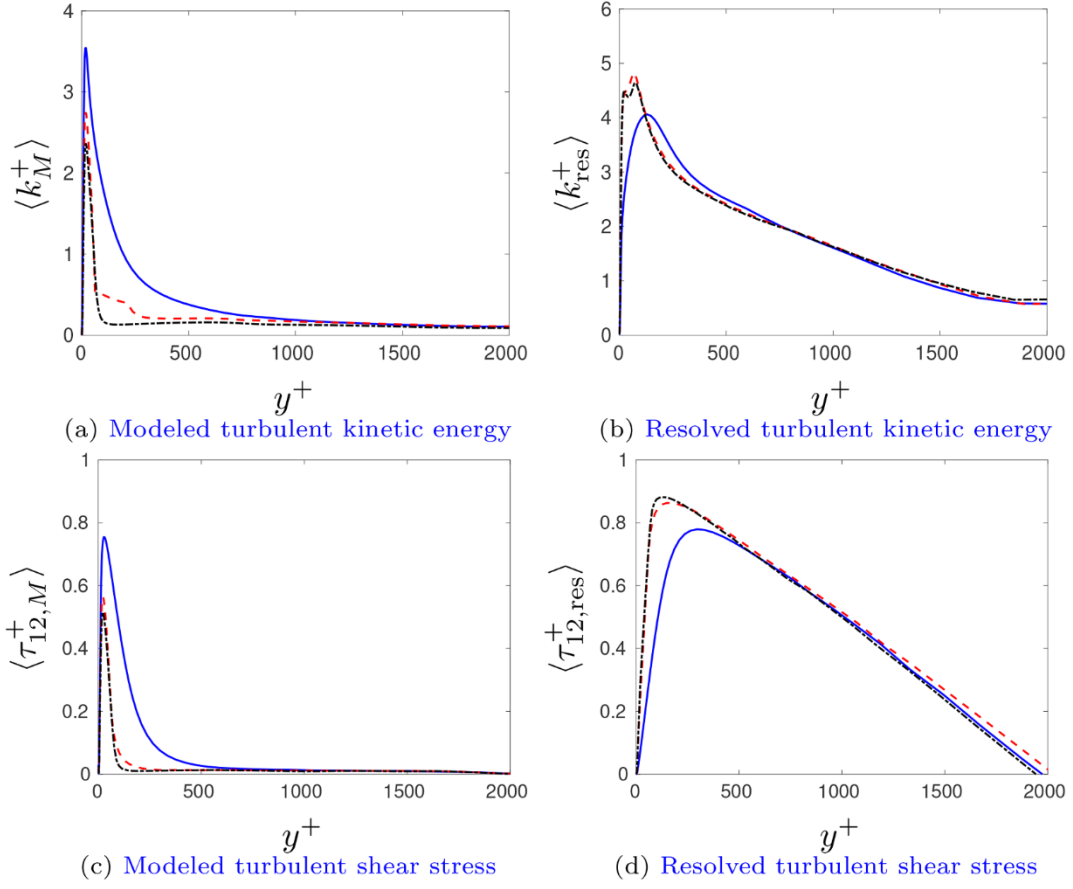


Fig. 7. Channel flow, $Re_\tau = 2000$. —: D-PANS; - - : IDD-PANS; - · - : IDDES; Markers: DNS (Lee and Moser, 2015).

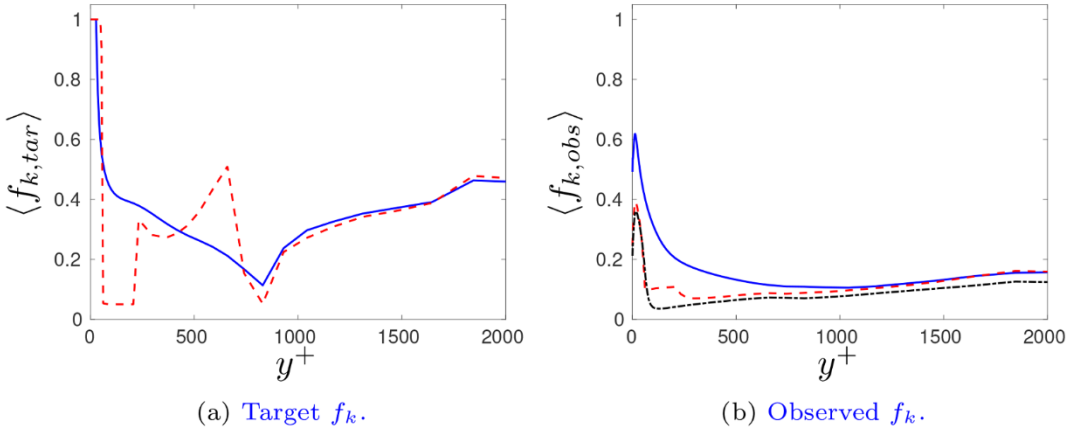


Fig. 8. Channel flow, f_k , $Re_\tau = 2000$. —: D-PANS; - - : IDD-PANS; - · - : IDDES.

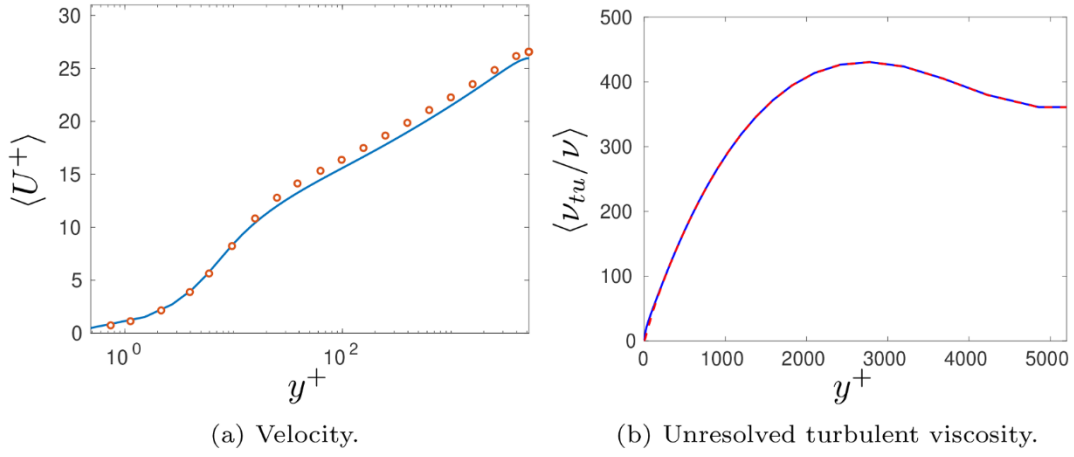


Fig. 9. Channel flow with steady initial conditions. $Re_\tau = 5200$. —: IDD-PANS; - - : 1D AKN RANS; Markers: DNS (Lee and Moser, 2015).

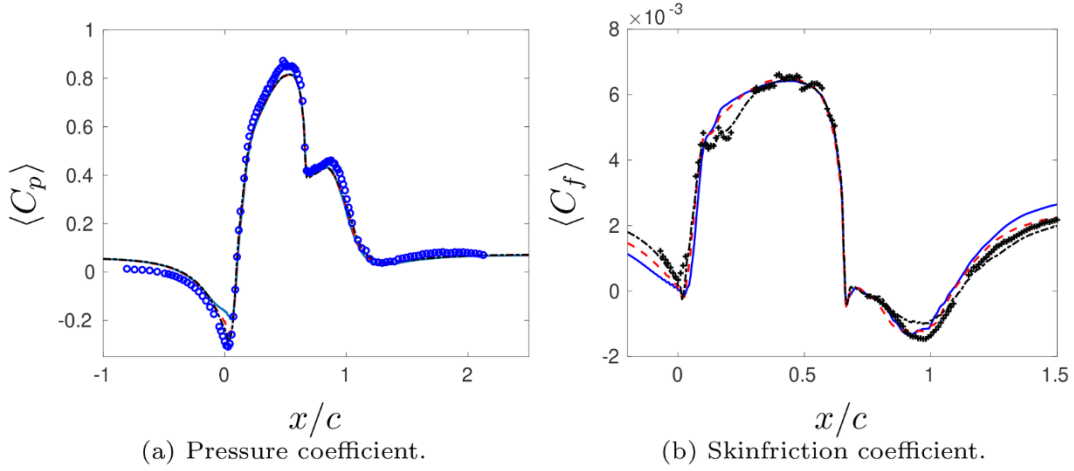


Fig. 10. Hump flow. Pressure coefficient and skinfriction. —: D-PANS; - - : IDD-PANS; - · - : IDDES; markers: Experiments (Greenblatt et al., 2004; Greenblatt et al., 2005).

but for the turbulent kinetic energy. As previously with the $Re_\tau = 5200$ channel case, the repartition between modeled and resolved scales is remarkably similar between IDD-PANS and IDDES, while D-PANS is clearly different. Moreover, τ_{12} is again overall more resolved than k . In other words, if we defined a τ_{12} -equivalent of f_k , called f_{12} , we would have $f_{12} < f_k$, especially toward the center of the channel.

Fig. 8(a) compares the target energy ratio $f_{k,tar}$ and between D-PANS and IDD-PANS, and Fig. 5(b) shows the profiles of the observed energy ratio $f_{k,obs}$ between D-PANS, IDD-PANS and IDDES. It is worth noticing that even though the $f_{k,tar}$ fields are not low enough to perform well-resolved LES in the sense of Pope (less than 20% of the energy must be modeled) in the full channel, the observed energy ratio $f_{k,obs}$ matches the aforementioned criterion, in more than 90% of the channel, for both IDDES and IDD-PANS. Moreover, it seems that D-PANS acts more like a basic hybrid RANS/LES, with a significant modeled part of energy near the wall, while IDD-PANS and IDDES seem to rather adopt the desired behaviour of wall modeled LES. Another interesting fact is that IDD-PANS and D-PANS exhibit similar $f_{k,tar}$ fields toward the middle of the channel, which results in a global accordance in $f_{k,obs}$, also with IDDES.

This tendency makes sense at first sight, but it was not observed with $Re_\tau = 5200$.

4.1.2. Steady case

In this case, the initial conditions are fully steady. The friction Reynolds Re_τ is 5200. Fig. 9(a) presents the mean velocity against the DNS results of Lee and Moser (2015). There is a good accordance with the DNS reference. Fig. 9(b) shows the unresolved eddy viscosity profile, compared with that obtained from a 1D RANS computation, using the same closure model (AKN). The profiles match perfectly, suggesting that in absence of fluctuating initial content, IDD-PANS is able, just like IDDES, to enforce a proper RANS mode. This is confirmed by the fact that IDDES gives $f_{k,tar} = 1$ (not shown).

4.2. Hump flow

The Reynolds number of the hump flow is $Re_c = 936\,000$, based on the hump length, $c = 1$, and the inlet mean velocity at the centerline, $U_{in,c}$. In the present simulations, the values of ρ , c and $U_{in,c}$ have been set

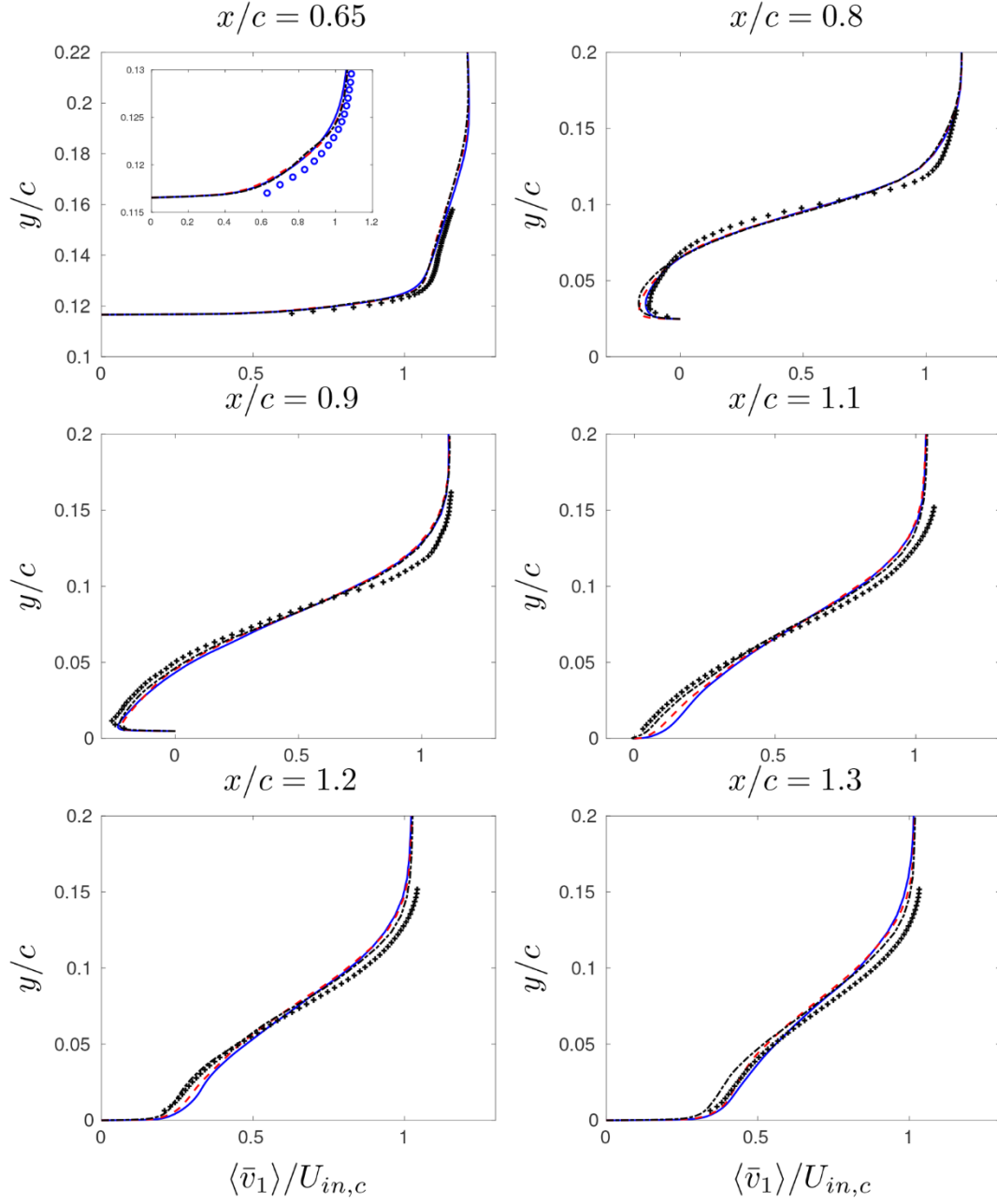


Fig. 11. Hump flow. Streamwise velocities. —: D-PANS; - - : IDD-PANS; - · - : IDDES; markers: Experiments (Greenblatt et al., 2004; Greenblatt et al., 2005).

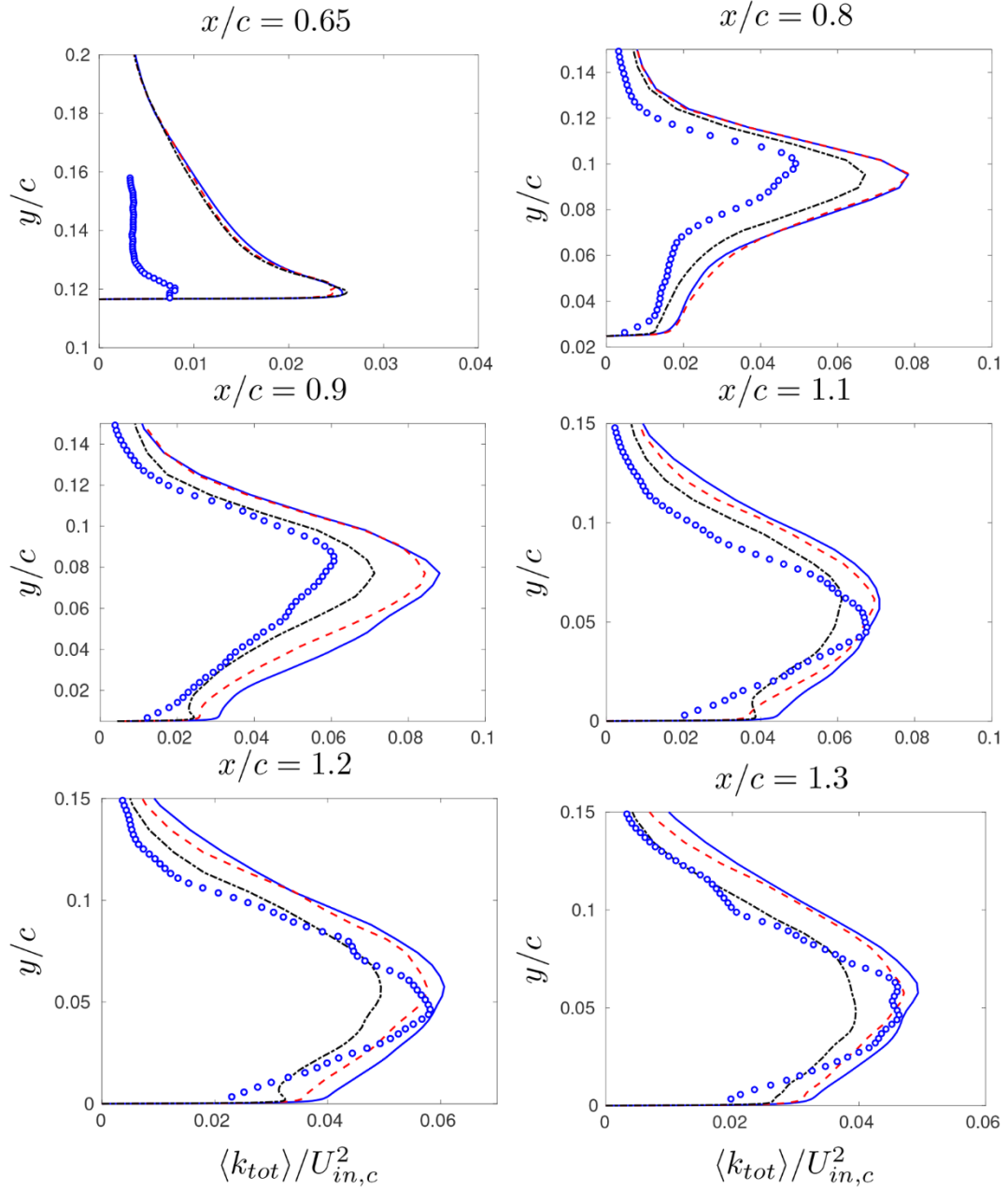


Fig. 12. Hump flow. Total turbulent kinetic energy. — : D-PANS; -- -- : IDD-PANS; $\text{-} \cdot \text{-}$: IDDES; markers: Experiments (Greenblatt et al., 2004; Greenblatt et al., 2005).

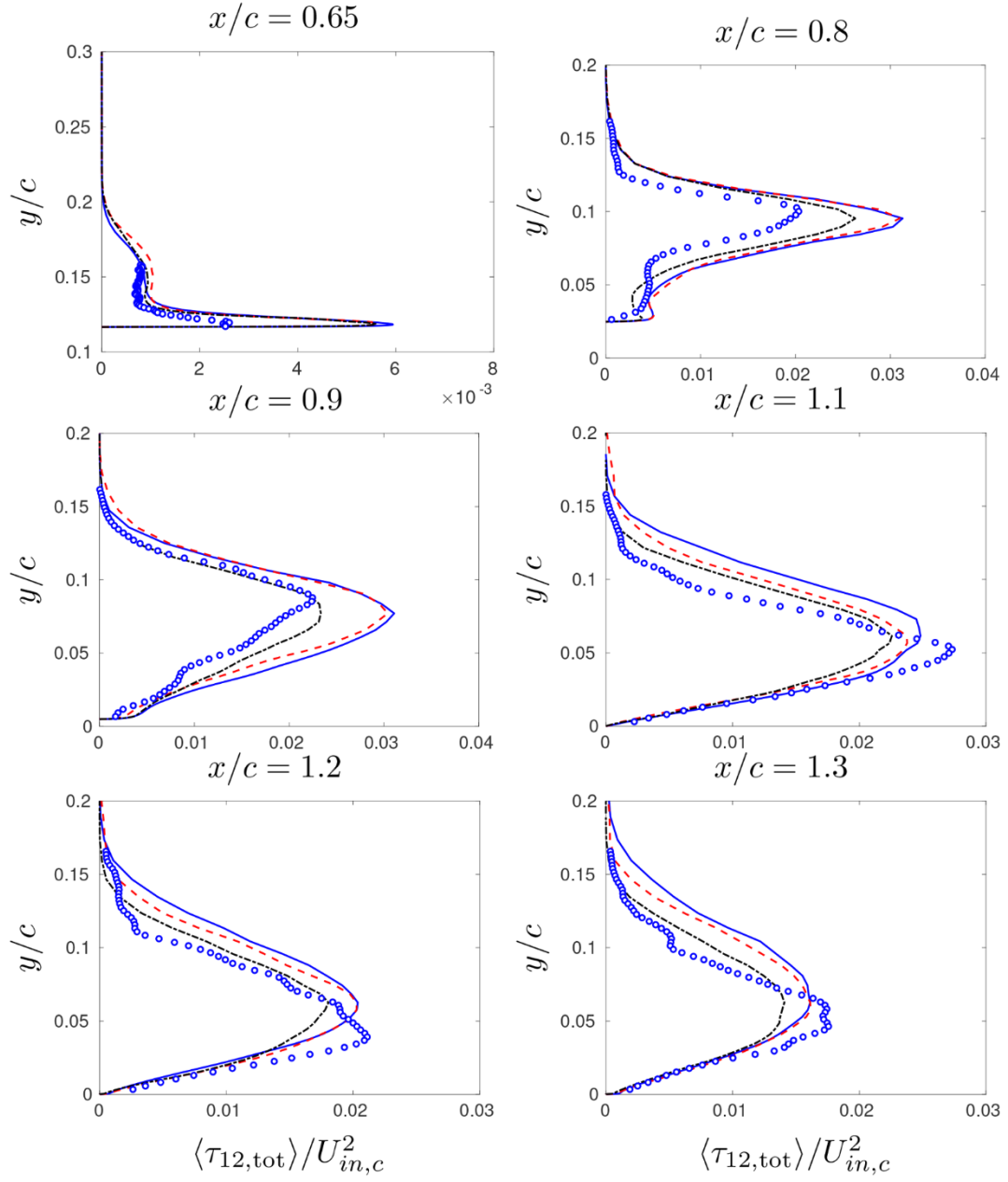


Fig. 13. Hump flow. Total turbulent shear stress τ_{12} . —: D-PANS; - - : IDD-PANS; - · - : IDDES; markers: Experiments (Greenblatt et al., 2004; Greenblatt et al., 2005).

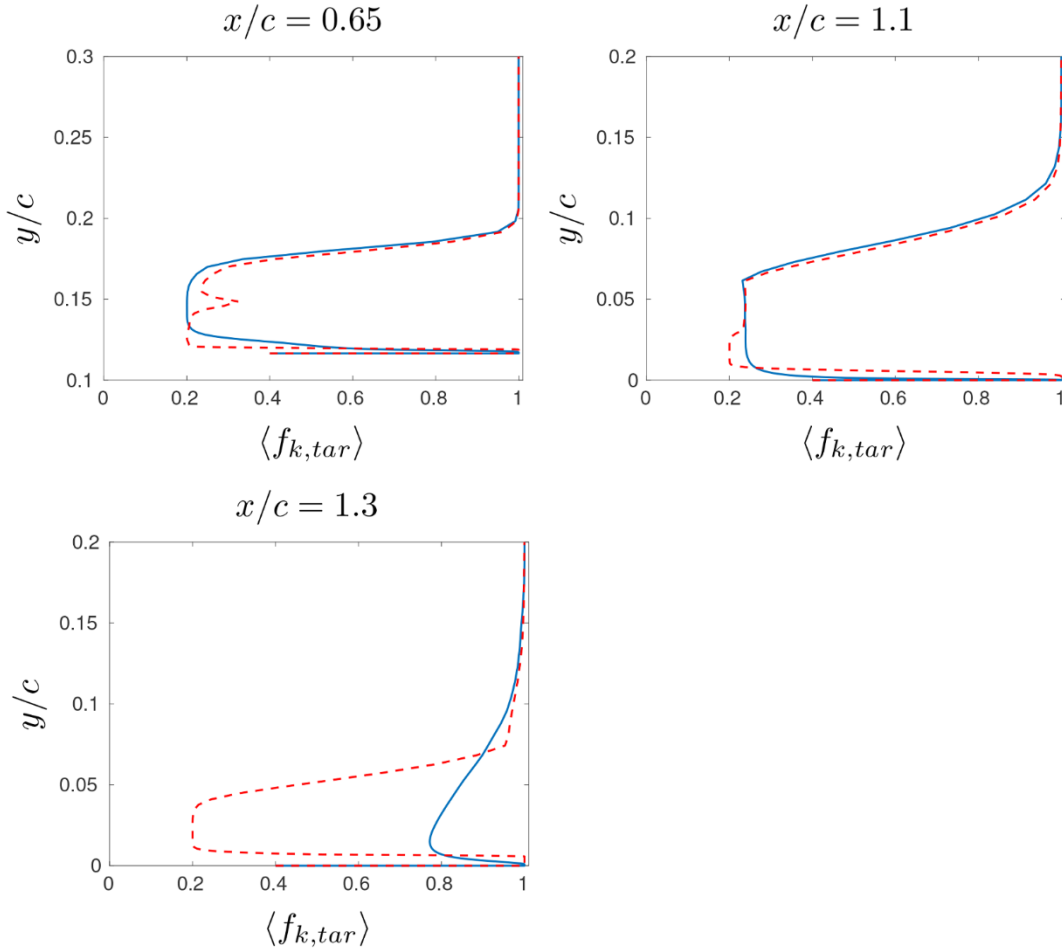


Fig. 14. Hump flow. $f_{k,tar}$. —: D-PANS; - - : IDD-PANS.

to unity. The configuration is given in Fig. 1. Experiments were conducted by Greenblatt et al. (2004) and Greenblatt et al. (2005). The maximum height of the hump, h , and the channel height, H , are given by $h/c = 0.128$ and $H/c = 0.91$, respectively. The mesh has $648 \times 108 \times 64$ cells and is taken from the NASA workshop.¹ The spanwise extent is set to $Z_{max}/c = 0.3$. Initially, a time step of $0.002c/U_{in,c}$ was used which worked fine for D-PANS and IDD-PANS; for IDDES, however, the simulation was numerically unstable and diverged. A smaller time step of $0.001c/U_{in,c}$ was chosen for all three turbulence models. The inlet is located at $x/c = -2.1$ and the outlet at $x/c = 4.0$. A periodic boundary condition is applied in the spanwise direction z . Therefore, this direction is considered statistically homogeneous.

The conditions (U , V , k and ε) are taken from a 2D RANS simulation with the same momentum thickness as the experimental velocity profiles. The AKN $k-\varepsilon$ turbulence model (Abe et al., 1994) is used coupled to the EARSM model (Wallin and Johansson, 2000). Synthetic isotropic fluctuations are superimposed on the 2D RANS velocity field. The synthetic fluctuations are scaled with the RANS shear stress profile. To reduce the inlet k , prescribed from 2D RANS, a commutation term $\partial f_k / \partial x$ is used. For more detail on inlet synthetic fluctuations and the commutation term, see Davidson (2016). For the sake of numerical stability, a lower limit of 0.2 is used when computing $f_{k,tar}$ from Eq. (47).

The simulations are initialized as follows (Davidson, 2019): first the

2D RANS equations are solved. Anisotropic synthetic fluctuations, $(\mathcal{V}'_i)_m$, are then superimposed to the 2D RANS field which gives the initial LES velocity field. In order to compute $(\mathcal{V}'_i)_m$, synthetic fluctuations, $v'_{i,synt}$, are computed plane-by-plane ($y-z$) in the same way as prescribing inlet boundary conditions. The synthetic fluctuations in the $y-z$ planes are coupled with an asymmetric space filter

$$(\mathcal{V}'_i)_m = a(\mathcal{V}'_i)_{m-1} + b(v'_{syn,i})_m \quad (50)$$

where m denotes the index of the x_1 location and $a = \exp(-\Delta x_1/L_{int})$ and Δx_1 and L_{int} denote the grid size and the integral length scale, respectively ($L_{int} = 0.2$).

Fig. 10(a) compares the profiles of the pressure coefficient C_p . The three models, IDDES, IDD-PANS and D-PANS offer very similar performance, except over the hump at $x/c = 0$, where D-PANS fails in predicting the strong longitudinal gradient of C_p , while IDD-PANS and IDDES succeed. Fig. 10(b) shows the skinfriction coefficient C_f profiles. IDDES gives a better agreement with experiment in the boundary layer ($x < 0$), whereas IDD-PANS shows a better agreement than IDDES and D-PANS in the recirculation region.

Fig. 11 shows the streamwise velocity profiles at several locations of the domain, starting from nearly the middle of the hump, to positions located downstream the hump, before and after reattachment. As expected for a flow exhibiting massive separation, the three approaches have a very similar behaviour, except downstream reattachment

¹ https://turbmodels.larc.nasa.gov/nasahump_val.html.

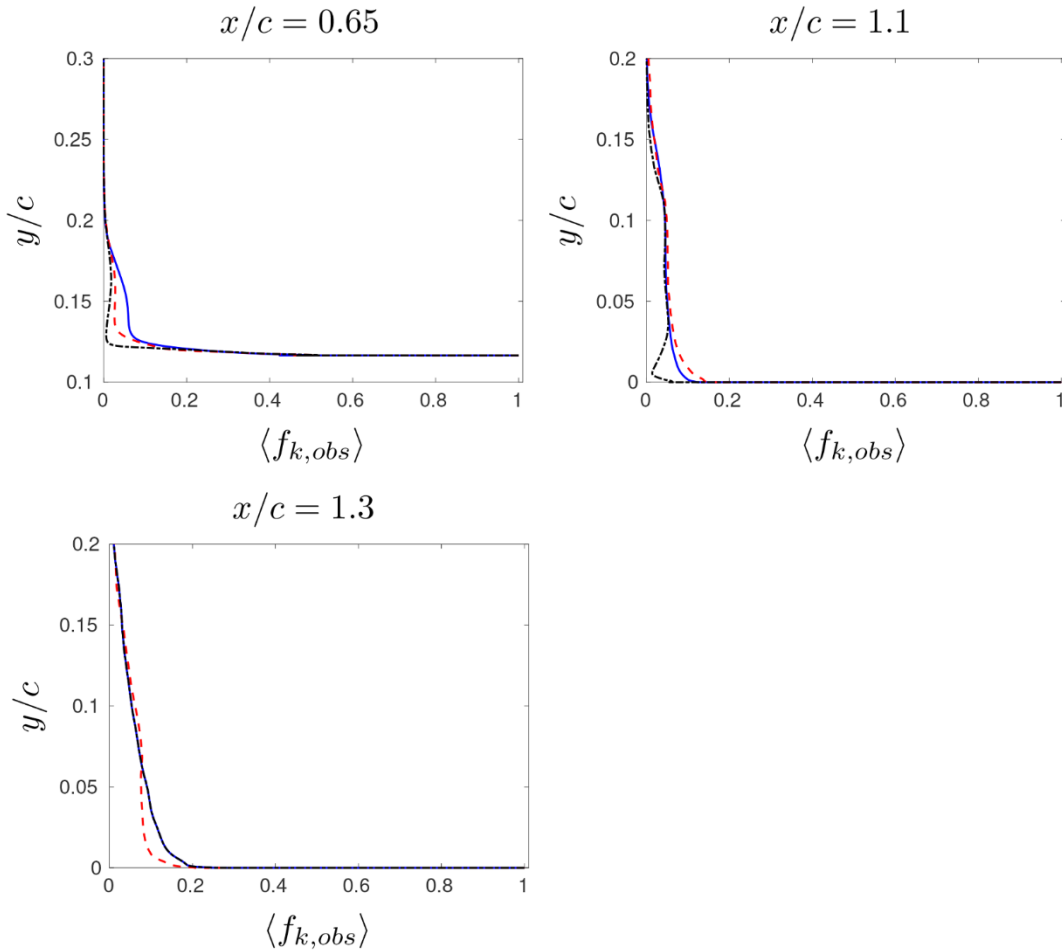


Fig. 15. Hump flow. $f_{k,obs}$. —: D-PANS; - - : IDD-PANS; - · - : IDDES.

($x/c \geq 1.1$), where IDD-PANS shows some superiority over D-PANS.

Figs. 12 (resp. 13) show the total turbulent kinetic energy (resp. shear stress τ_{12}) at the same six locations as above. Before reattachment ($x/c = 0.65, 0.8$ and 0.9), all three approaches overestimate k_{tot} and $\tau_{12,tot}$, especially before separation ($x/c = 0.65$). This might be due to poor resolution of the thin accelerating boundary layer at the upstream part of the hump. One can also notice that there is an overall surprisingly good agreement between IDD-PANS and D-PANS, rather than with IDDES, on those total quantities. They both capture well the peaks of k_{tot} downstream reattachment, but not those of $\tau_{12,tot}$, also they do better than IDDES. On the other hand, all three approaches fail at predicting k_{tot} in the near wall region, but perform better on $\tau_{12,tot}$, especially downstream reattachment ($x/c \geq 1.1$).

Fig. 14 compares the targetted values of the energy ratio, $f_{k,tar}$, between IDD-PANS and D-PANS, taken at three locations: slightly before separation ($x/c = 0.65$), and downstream reattachment ($x/H = 1.1$ and $x/H = 1.3$). The shape of the IDD-PANS $f_{k,tar}$ is somewhat more complex than that of D-PANS. Again, this suggests that IDD-PANS inherits the fact that IDDES is more elaborate than DES, as observed for the channel flow. However, the overall values of $f_{k,tar}$ are similar in IDD-PANS and D-

PANS, except at $x/c = 1.3$ where the near-wall region is treated nearly in RANS mode by D-PANS ($f_{k,tar} \approx 0.8$), while better resolved by IDD-PANS ($f_{k,tar} \approx 0.2$ at its lowest).

Fig. 15 shows profiles of the observed energy ratio, $f_{k,obs}$, compared between IDDES, D-PANS and IDD-PANS, at the same locations as in Fig. 14. Surprisingly, the profiles are very close to each other. The small discrepancies observed, occur in the near wall region. But the most important observation is that, in spite of a moderately resolved input $f_{k,tar}$, the $f_{k,obs}$ are very low, suggesting an overall LES mode. This is caused by the fact that the large resolved scales dominate this out-of-equilibrium flow, as suggested by Figs. 16 (resp. 17). Those latter show the repartitions between modeled and resolved parts of the turbulent kinetic energy (resp. shear stress) at the same three locations. They clearly show that at all of the three locations, the modeled k and τ_{12} are significantly smaller than their resolved counterparts. Accordingly, the latter exhibit a very qualitative agreement, through similar shapes and peak locations, however with various values. In the near wall region and downstream reattachment, the three approaches exhibit significantly different behavior of the modeled quantities, particularly for k_M . This is counterintuitive, since the near wall region is the closest to the

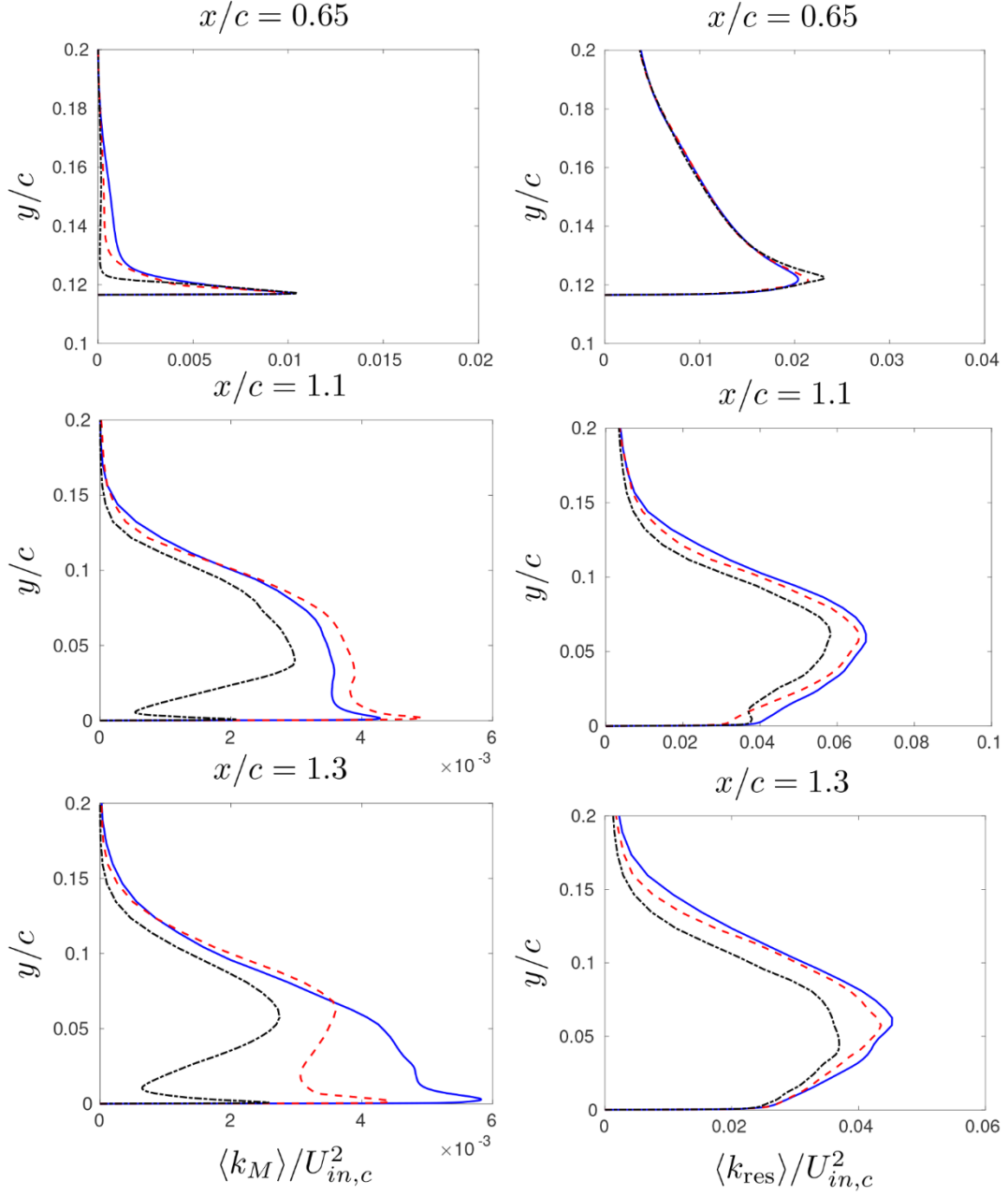


Fig. 16. Hump flow. Turbulent kinetic energy: modeled part (left) and resolved part (right). —: D-PANS; - - : IDD-PANS; · · · : IDDES.

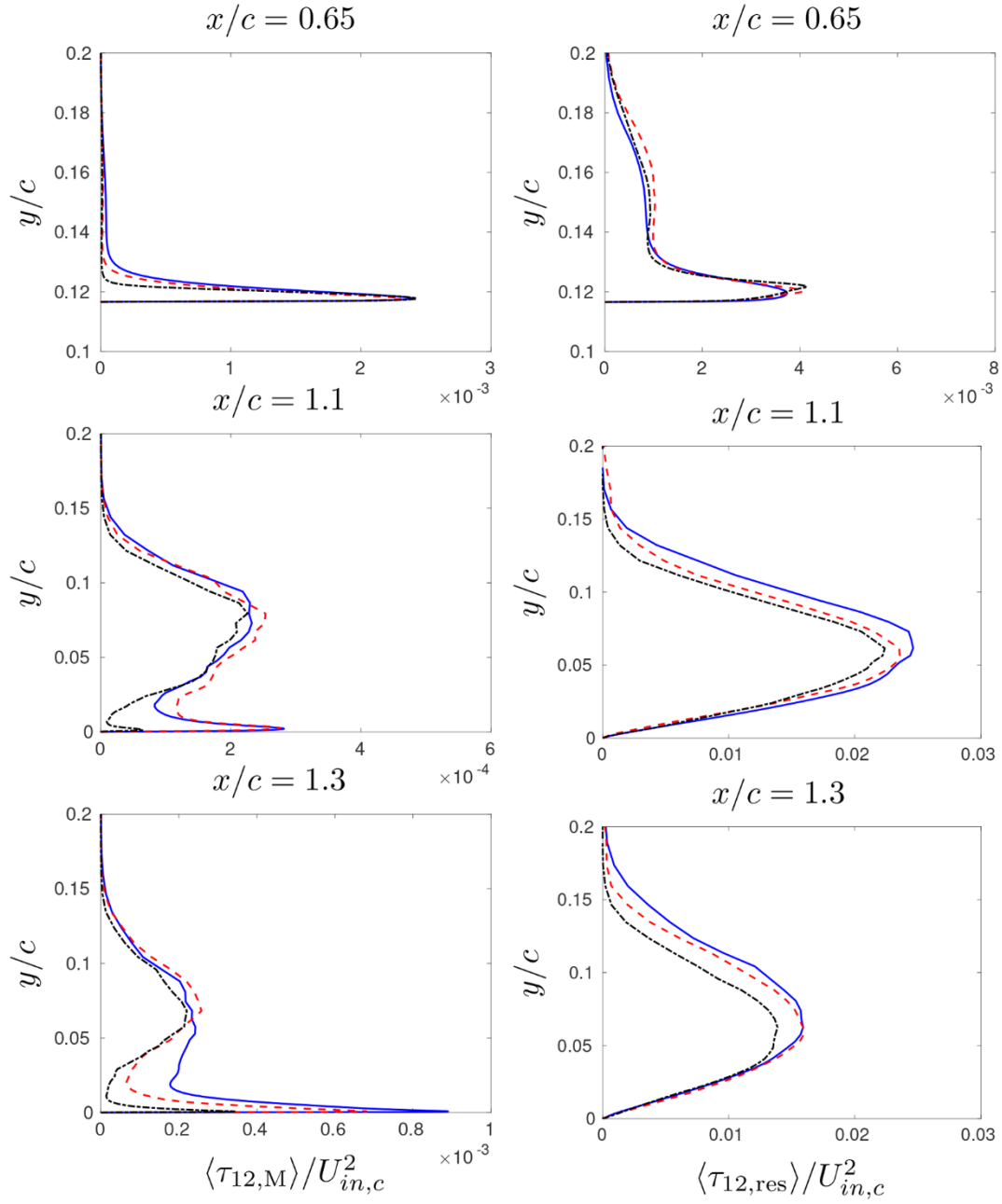


Fig. 17. Hump flow. Turbulent shear stress: modeled part (left) and resolved part (right). —: D-PANS; - - : IDD-PANS; - · - : IDDES.

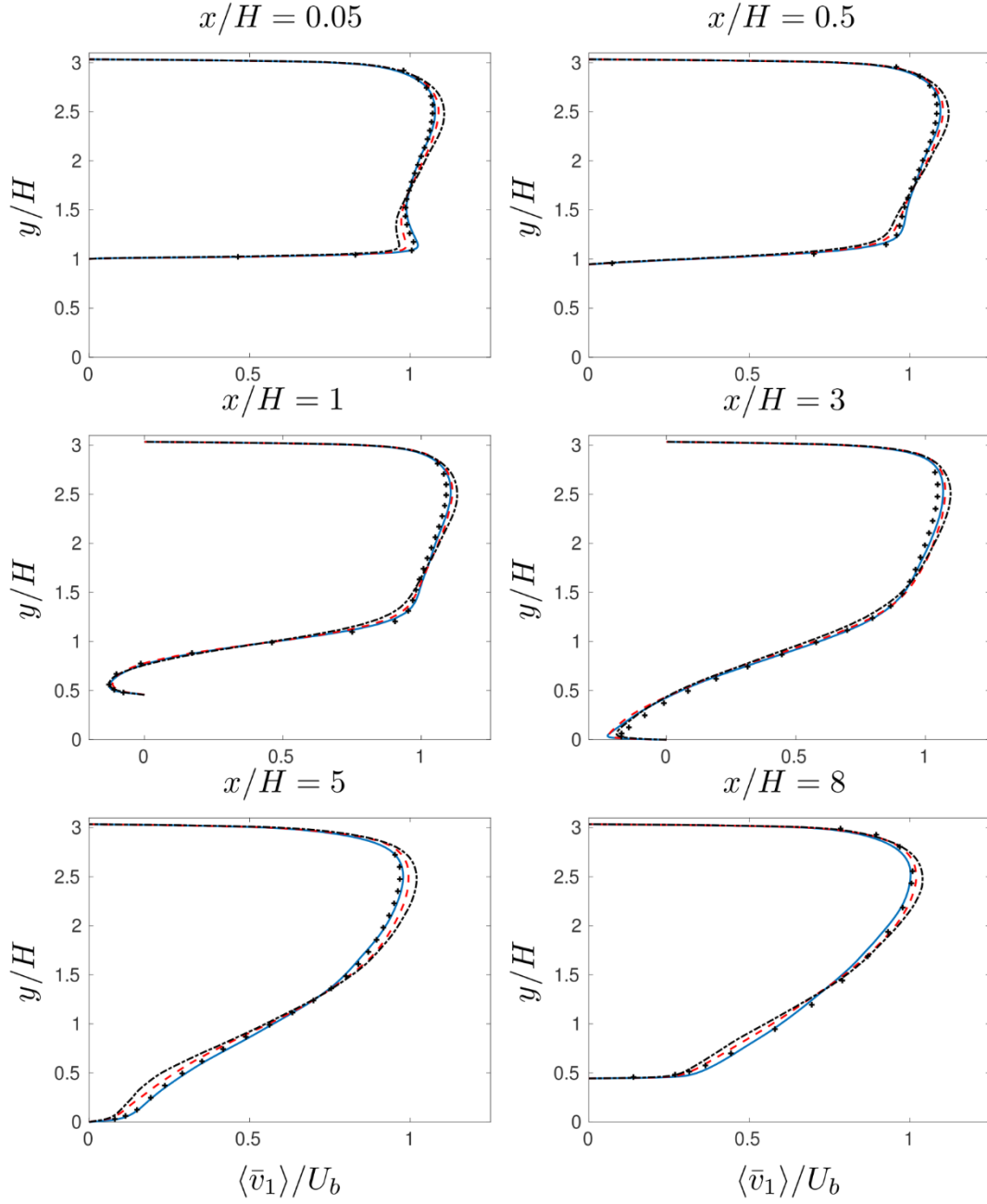


Fig. 18. Hill flow. Velocities. —: D-PANS; - - : IDD-PANS; - · - : IDDES; markers: LES (Breuer et al., 2009).

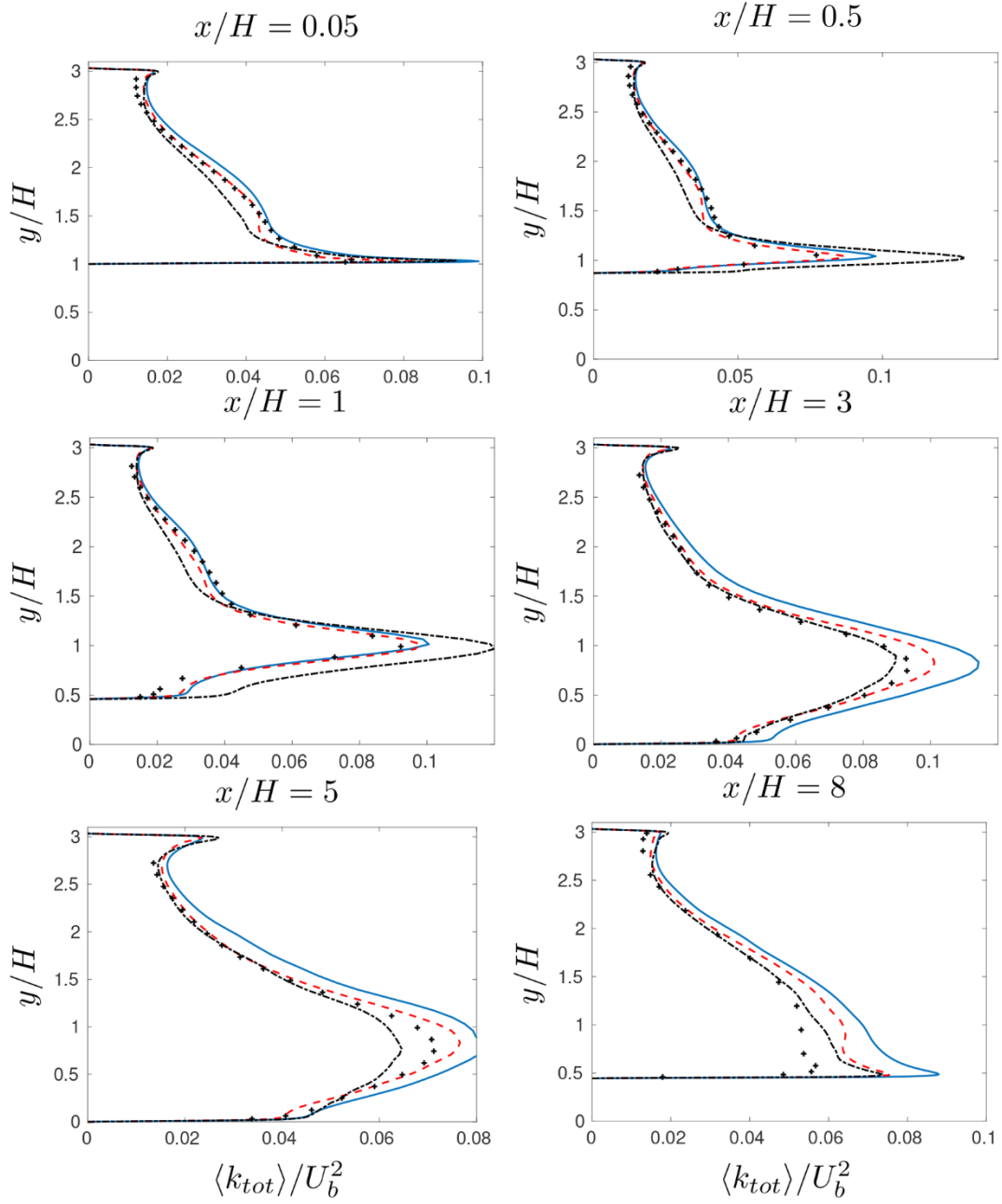


Fig. 19. Hill flow. Total turbulent kinetic energy. —: D-PANS; - - : IDD-PANS; - · - : IDDES; markers: LES (Breuer et al., 2009).

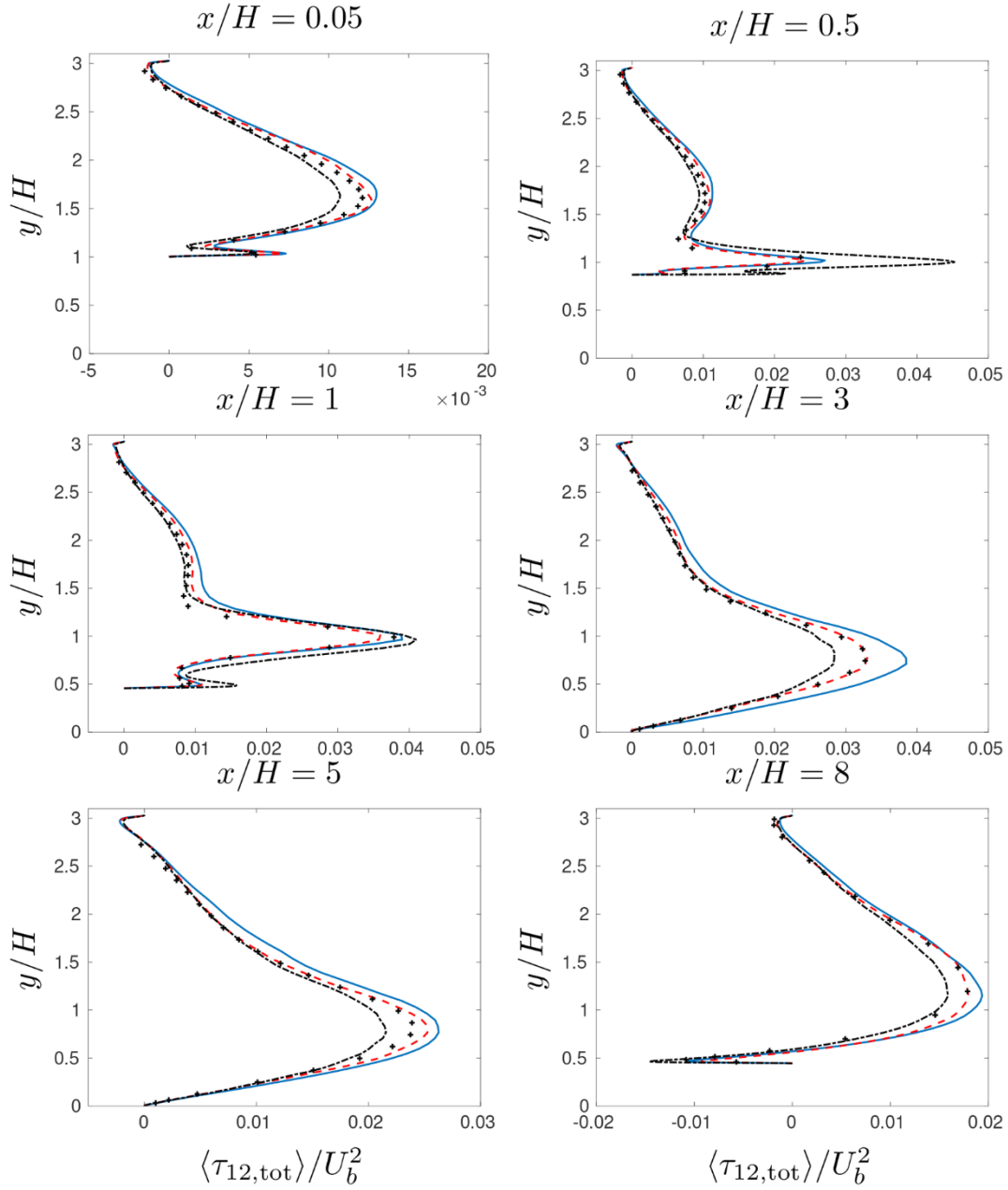


Fig. 20. Hill flow. Total turbulent shear stress. —: D-PANS; - - : IDD-PANS; - · - : IDDES; markers: LES (Breuer et al., 2009).

RANS mode, thus the three models should behave more similarly, since they share the same parent RANS closure. Finally, before separation ($x/c = 0.65$), one can see that the three approaches agree quite well, regarding modeled as well as resolved quantities.

4.3. Hill flow

The domain is shown in Fig. 2. The size of the domain is $9H \times 3.035H \times 4.5H$ in the streamwise (x), wall-normal (y) and span-wise direction (z), respectively. The grid has $160 \times 80 \times 32$ cells in the x , y and z direction. Periodic boundary conditions are used in the x and z directions. The z direction is considered statistically homogeneous. Slip conditions are prescribed at the upper wall. The Reynolds number is $Re = 10600$ based on the hill height and the bulk velocity U_b at the top

of the hill. An initial velocity field is prescribed from a 2D RANS solution with the correct bulk Reynolds number. Furthermore, the same technique for synthetic turbulence as for the hump flow (see Eq. 50), is used to add initial fluctuations. The bulk velocity is then kept constant by adjusting β in Eq. 48 at each time step by ensuring that the sum of the forces at the wall (wall shear stress and pressure on the lower wall) balances the driving pressure gradient (Irannezhad, 2006; Orlandi, 2000, Section 4.5).

Fig. 18 shows the streamwise velocity profiles at several locations of the domain: on the top of the hill before separation ($x/H = 0.05$ and 0.5), in the expanded area after separation $x/H = 1$, on the bottom of the domain before and after reattachment ($x/H = 3$ and 5), and in the constricted area ($x/H = 8$). As observed in the previous section with the hump flow, the three approaches have a very similar behaviour, except

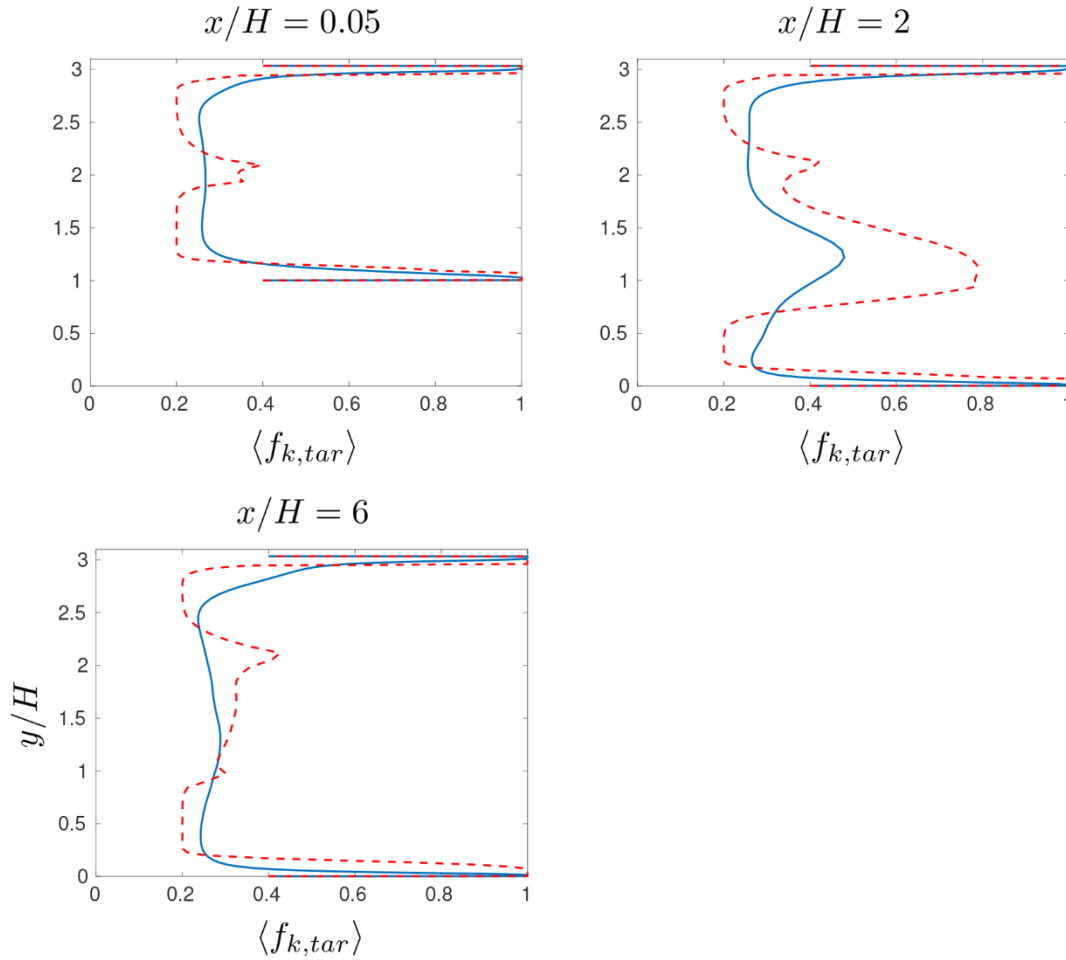


Fig. 21. Hill flow. $f_{k,tar}$. —: D-PANS; - - : IDD-PANS.

downstream reattachment ($x/H \geq 5$), where IDD-PANS is closer to IDDES than D-PANS.

Figs. 19 and 20 show the total turbulent kinetic energy (resp. shear stress τ_{12}) at the six same locations as above. The three hybrid RANS/LES approaches exhibit various behaviors in this flow, but they reasonably capture peaks and inflection points. IDD-PANS seems in overall good agreement with the reference LES of Breuer et al. (2009), especially regarding $\tau_{12,tot}$. The performance of IDDES is more debatable, especially upstream reattachment. Surprisingly, D-PANS does not perform as well as the other two approaches on k_{tot} , further downstream separation $x/H \geq 3$, but performs reasonably good on $\tau_{12,tot}$.

Fig. 21 compares the targetted values of the energy ratio, $f_{k,tar}$, between IDD-PANS and D-PANS, at three locations: on the top of the hill ($x/H = 0.05$), in the recirculation bubble ($x/H = 2$) and downstream reattachment ($x/H = 6$). As observed with the other two flows, it is worth noticing that the shape of the IDD-PANS $f_{k,tar}$ profile is slightly more complex than that of D-PANS. Again, this suggests that IDD-PANS inherits the fact that IDDES is more elaborate than DES. However, the overall values of $f_{k,tar}$ are similar in IDD-PANS and D-PANS, except at $x/H = 2$ where the region near $y/H = 1$ is treated nearly in RANS mode by IDD-PANS ($f_{k,tar} \approx 0.8$), while better resolved by D-PANS ($f_{k,tar} \approx 0.45$).

Fig. 22 shows profiles of the observed energy ratio, $f_{k,obs}$, compared

between IDDES, D-PANS and IDD-PANS, at the same locations as in 21. Interestingly, the $f_{k,obs}$ profiles do not vary much along the domain. The small discrepancies observed are consistent with those observed with modeled k on Fig. 23 and occur mainly close to the walls.

Figs. 23 (resp. 24) show repartitions between modeled and resolved parts of the turbulent kinetic energy (resp. shear stress) at the same three locations as above. As for the hump flow, one can notice that at all of the three locations, the modeled k and especially τ_{12} are significantly smaller than their resolved counterparts, which makes sense for a flow exhibiting massive separation, dominated by the large-scale turbulent motion. But contrary to the hump flow, there is no qualitative agreement between the three hybrid RANS/LES approaches, regarding resolved quantities, except on peak and inflection point locations. This is also observed with modeled quantities, however in a less clear way.

Fig. 25(a)–(c) show isocontours of the Q -criterion defined by:

$$Q = \frac{1}{2} (\bar{\mathbf{S}} : \bar{\mathbf{S}} - \bar{\mathbf{W}} : \bar{\mathbf{W}}) \quad (51)$$

with

$$\bar{\mathbf{S}} = \frac{1}{2} (\nabla \bar{\mathbf{v}} + \nabla^T \bar{\mathbf{v}}) \text{ and } \bar{\mathbf{W}} = \frac{1}{2} (\nabla \bar{\mathbf{v}} - \nabla^T \bar{\mathbf{v}}) \quad (52)$$

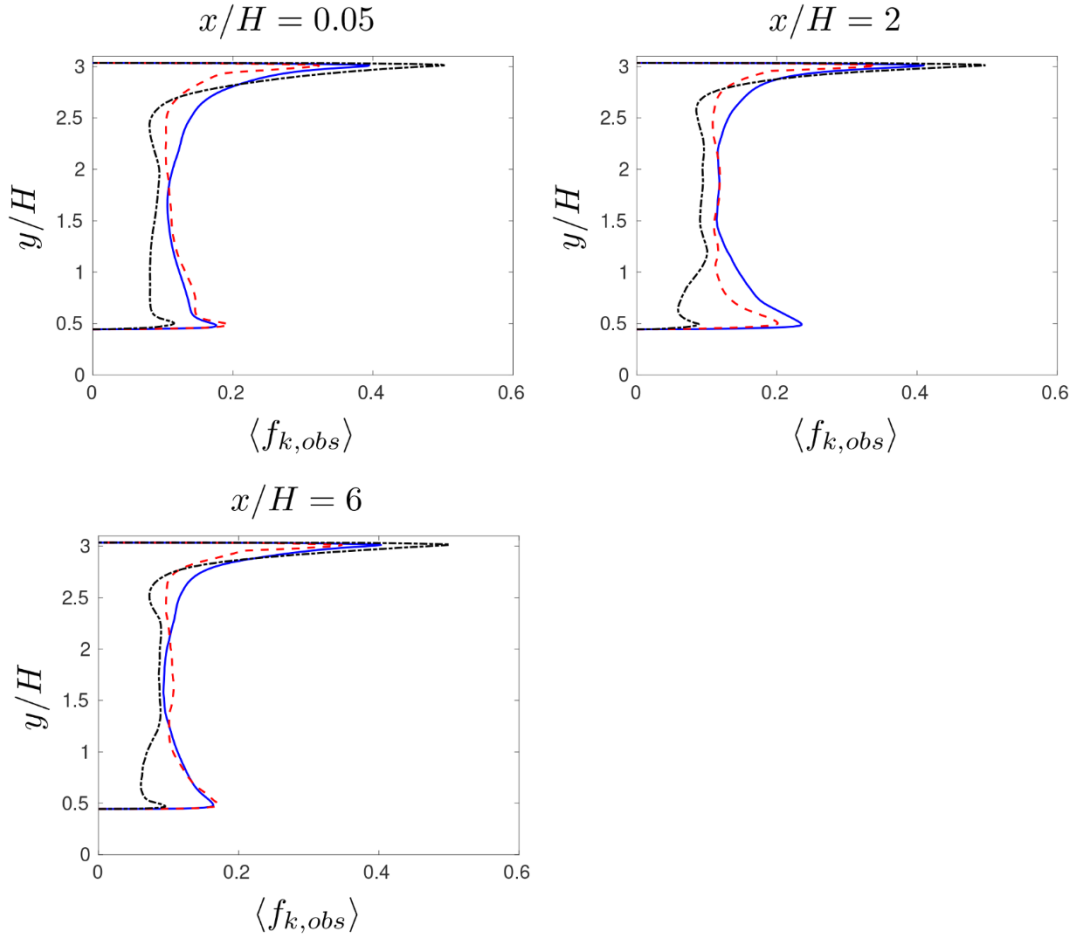


Fig. 22. Hill flow. $f_{k,obs}$. —: D-PANS; - - : IDD-PANS; - · - : IDDES.

Q is normalized by relevant time scales, and colored by the instantaneous velocity magnitude. Fig. 25(a) shows IDD-PANS isocontours of Q for the lower half of the channel flow at $Re_\tau = 5200$. Fig. 25(b) shows IDD-PANS isocontours of Q for the hill flow, and Fig. 25(c) for the hump flow. Quite intuitively, one can observe the finest structures in the hump flow. The hill flow, also dominated by the large-scale motion, which is reasonably resolved, exhibits fine streaks as well. The channel flow, which is the least resolved of the three cases studied here, logically exhibits the coarsest streaks.

5. Concluding remarks

A novel version of PANS, able to behave as IDDES, has been derived theoretically, following the analysis of Friess et al. (2015) leading to a low-order statistical equivalence they called “H-equivalence”. A quantitative relationship has been determined between their respective cut-off functions, namely f_k for PANS and ψ for IDDES, in the framework of stationary and inhomogeneous flows, at sufficient high Reynolds number, such that the resolved dissipation rate can be assumed negligible compared to its unresolved counterpart. In the present paper, the analysis is limited to one turbulent closure model, but can be applied to any other.

Though the scale partitioning is less rigorously equivalent than for PITM and DES (see Friess et al., 2015), the main features of IDDES are qualitatively mimicked by the present approach. First, the log-layer mismatch, frequent in attached boundary layer flows, is no longer observed. The IDD-PANS approach gives a better prediction of the mean

streamwise velocity than D-PANS, and is very close to the profile predicted by IDDES. Secondly, the approach is able to respond to non-fluctuating inlet or initial conditions, thus able to behave in a proper RANS mode when needed. In particular, the present IDD-PANS approach is able to set the target energy ratio $f_{k,tar}$ to 1 when no turbulent inlet or initial content is provided. However, it is worth noticing that for the hump flow, IDD-PANS turned out to be more stable than IDDES, since the timestep had to be reduced for the latter.

Nevertheless, IDD-PANS does not perfectly match IDDES. The discrepancies between IDDES and IDD-PANS may be due to unadapted assumptions in the derivation of the equivalence criterion. In particular, the assumption that the relative variation of modeled turbulent kinetic $\delta k_M/k_M$ is constant throughout the fluid domain, is very strong and not really suitable for flows where f_k exhibits strong gradients. Moreover, the dissipation rate ε is assumed to be totally modeled (i.e. $f_\varepsilon = 1$), since at high Reynolds numbers, energetic and dissipative scales are sufficiently separated. But (i) near walls, the local Reynolds number is smaller, such that dissipation may occur at resolved scales and (ii) with a sufficiently fine mesh, e.g. in a true LES mode, resolved dissipation must be non negligible. Besides, it is worth noticing that the equivalence between IDDES and IDD-PANS is stronger in the case of the channel flow, than for the two other cases studied here. This can be explained by the fact that the initial “H-equivalence” in Friess et al. (2015) was derived for equilibrium flows. The hump and hill flows exhibit massive separation, and thus fall out of this framework.

Further work will focus on calibrating IDD-PANS for other turbulent closures like $k-\omega$, and will be tested with explicit algebraic-like models

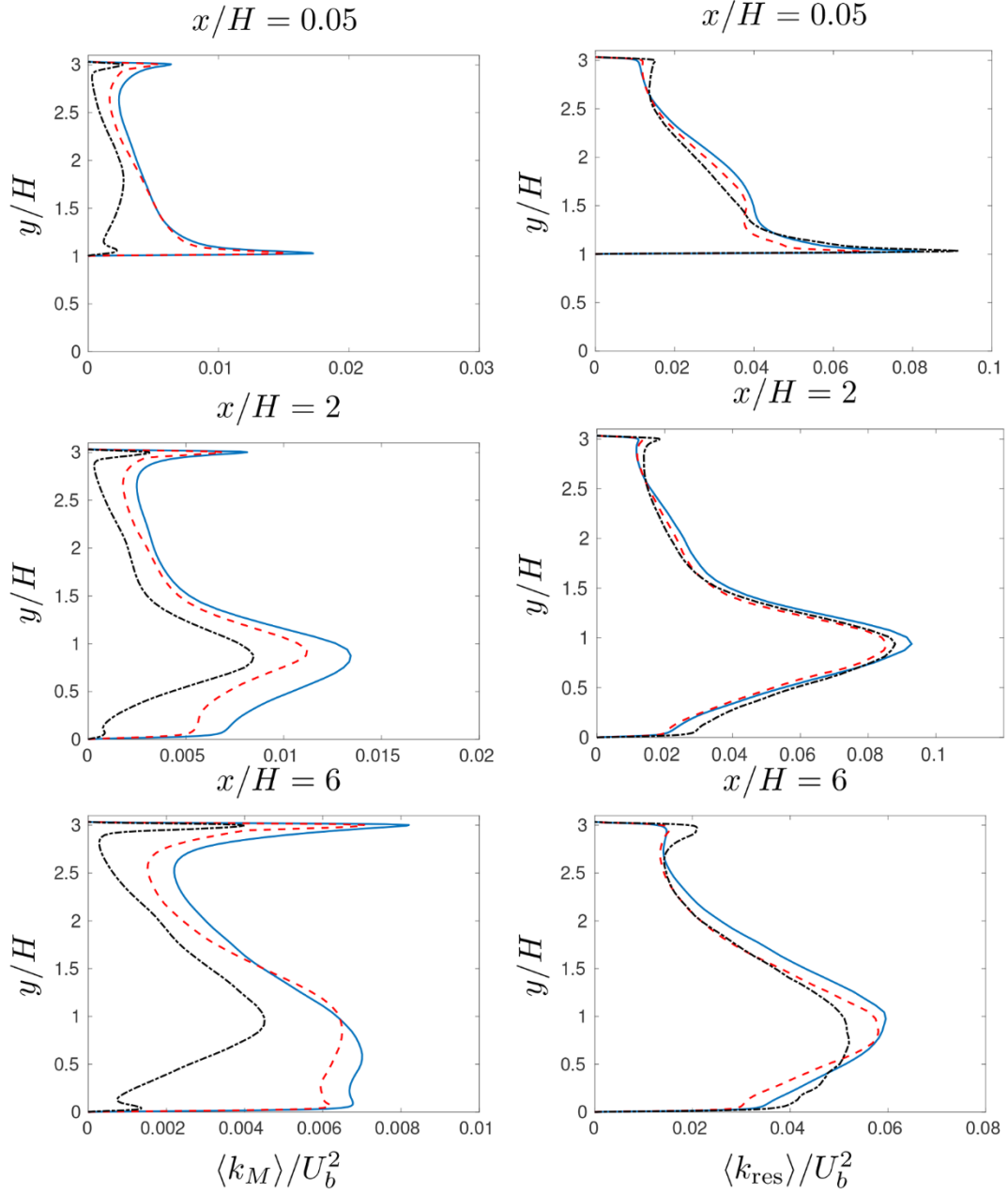


Fig. 23. Hill flow. Turbulent kinetic energy: modeled part (left) and resolved part (right). —: D-PANS; - - : IDD-PANS; - · - : IDDES.

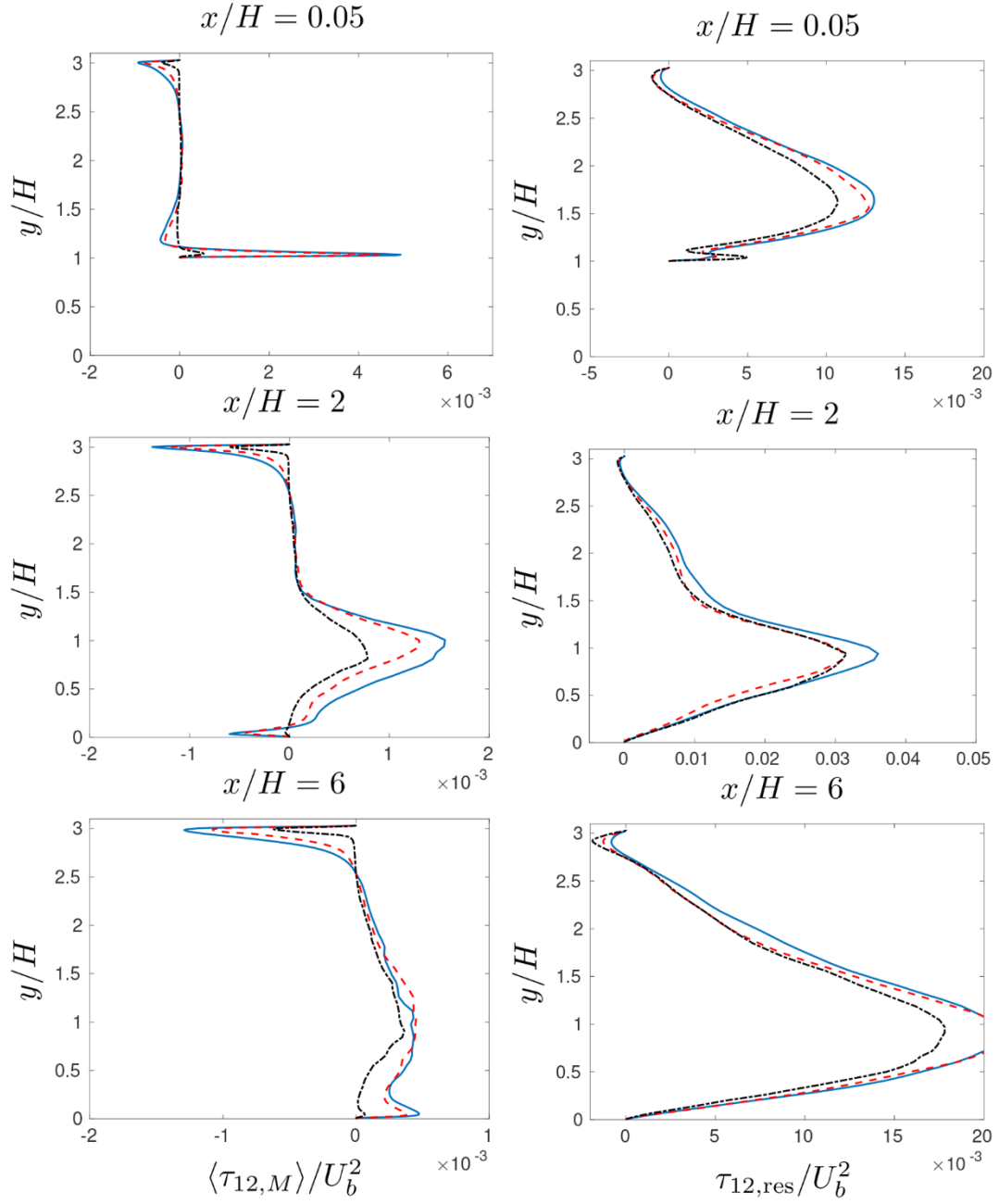


Fig. 24. Hill flow. Turbulent shear stress: modeled part (left) and resolved part (right). —: D-PANS; - - : IDD-PANS; - · - : IDDES.

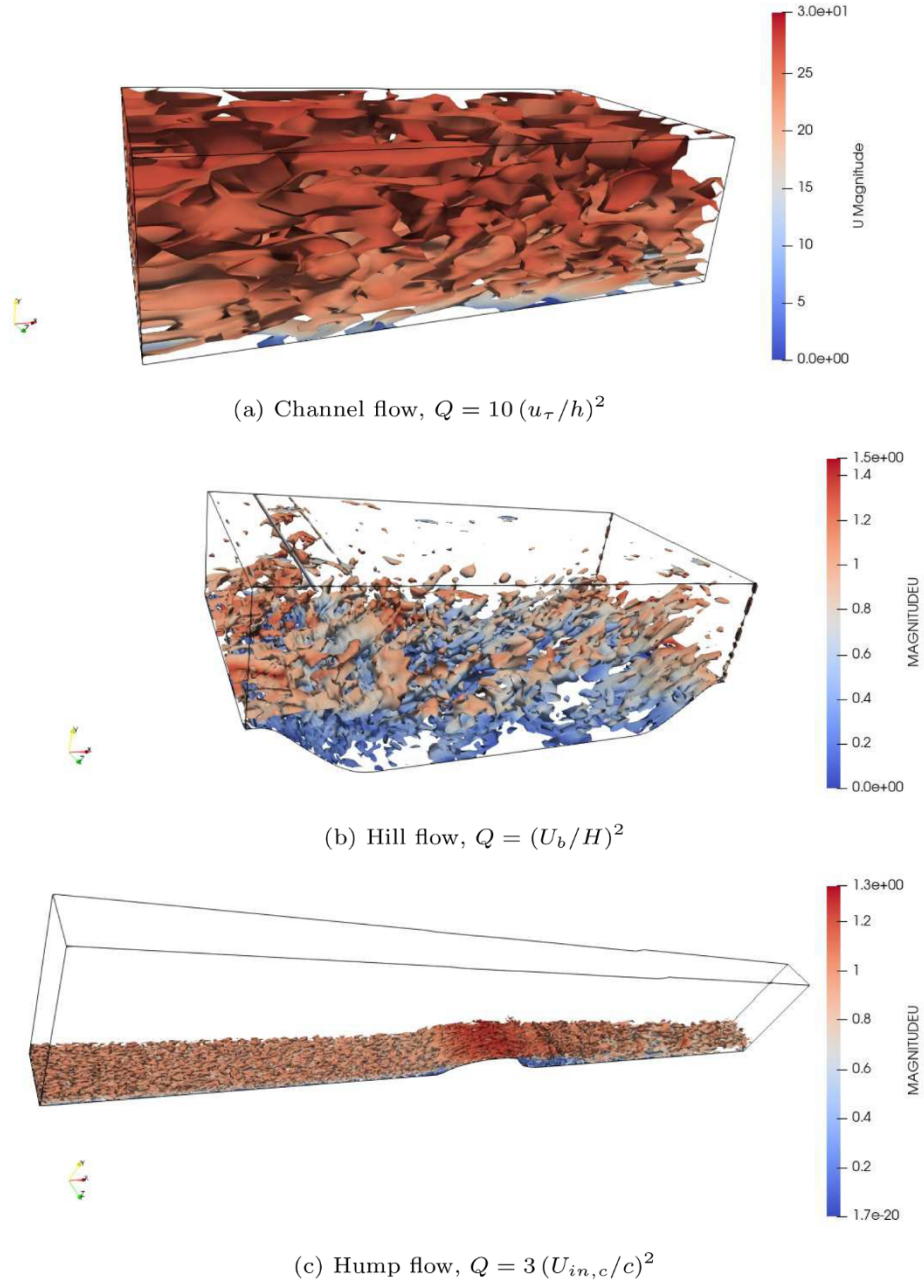


Fig. 25. IDD-PANS: isocontours of Q -criterion colored by respective instantaneous velocity magnitude.

as well. The effect of accounting for $f_\varepsilon \neq 1$ will be investigated as well.

CRediT authorship contribution statement

Christophe Friess: Conceptualization, Methodology, Formal analysis, Investigation, Writing - original draft, Visualization. **Lars Davidson:** Software, Validation, Formal analysis, Investigation, Resources,

Data curation, Writing - review & editing, Visualization.

Declaration of Competing Interest

The authors declare that they have no known competing financial interests or personal relationships that could have appeared to influence the work reported in this paper.

Appendix A. Calculation of the low-Reynolds correction Ψ

Here we detail the derivation of the low Reynolds number correction Ψ entering Eq. (8). To that aim, we follow the methodology explained in Arvidson et al. (2014).

The function Ψ is introduced so that the unresolved eddy viscosity ν_{tu} keeps a Smagorinsky-like shape, even at low Reynolds number, i.e.:

$$\nu_{tu} = C^2 \Delta^2 S \quad (\text{A.1})$$

where $C = \Psi C_{DES}$ is a constant, independent of the ratio ν_{tu}/ν . In other words, the role of Ψ is to de-activate the damping functions.

Let us consider the IDDES system $k_u - \varepsilon_u$ (Eq. (3)) involving the damping functions f_μ and f_2 given by Eq. (2). We define $S^2 = 2\bar{s}_{ij}\bar{s}_{ij}$. In that case, assuming local equilibrium between production and destruction terms in the transport equations for k_u and ε_u respectively yields :

$$\nu_{tu} S^2 = \frac{k_u^{3/2}}{\Psi C_{DES} \Delta} \quad (A.2)$$

$$\nu_{tu} S^2 = \frac{C_{\varepsilon 2} f_2 \varepsilon_u}{C_{\varepsilon 1}} \quad (A.3)$$

The unresolved dissipation ε_u can be eliminated from Eq. (A.3) by linking it to ν_{tu} and k_u :

$$\nu_{tu} = C_\mu f_\mu \frac{k_u^2}{\varepsilon_u} \Rightarrow \varepsilon_u = C_\mu f_\mu \frac{k_u^2}{\nu_{tu}} \quad (A.4)$$

Putting Eqs. (A.4) and (A.3) together yields:

$$\nu_{tu} S^2 = \frac{C_{\varepsilon 2} f_2 C_\mu f_\mu k_u^2}{C_{\varepsilon 1} \nu_{tu}} \Rightarrow k_u = \nu_{tu} S \sqrt{\frac{C_{\varepsilon 1}}{C_{\varepsilon 2} C_\mu f_\mu f_2}} \quad (A.5)$$

And if we use Eq. (A.5) to express k_u in Eq. (A.2), we obtain:

$$\nu_{tu} = \underbrace{\left(\frac{C_{\varepsilon 2} C_\mu f_\mu f_2}{C_{\varepsilon 1}} \right)^{3/2} \Psi^2 C_{DES}^2 \Delta^2 S}_{C^2} \quad (A.6)$$

Now, to make C independant of the damping functions f_μ and f_2 , we must have:

$$\Psi^2 = (f_\mu f_2)^{-3/2} \Rightarrow \Psi = (f_\mu f_2)^{-3/4} \quad (A.7)$$

It is worth noticing that this calibration of Ψ is performed only for IDDES, not for IDD-PANS explicitly. Indeed, through Eq. (47), the parameter f_k inherits all (ID)DES features, thus the low Reynolds number correction Ψ .

References

- Abe, K., Kondoh, T., Nagano, Y., 1994. A new turbulence model for predicting fluid flow and heat transfer in separating and reattaching flows – 1. Flow field calculations. *International Journal of Heat Mass Transfer* 37 (1), 139–151.
- Arvidson, S., Davidson, L., Peng, S.-H., 2014. Hybrid RANS-LES modeling using a low-Reynolds-number $k-\omega$ based model. In: *AIAA Science and Technology Forum and Exposition*, AIAA paper 2014-0225, Maryland, 13–17 January, 2014.
- Breuer, M., Peller, N., Rapp, Ch., Manhart, M., 2009. Flow over periodic hills – numerical and experimental study in a wide range of Reynolds numbers. *Computers & Fluids* 38, 433–457.
- Chaouat, B., Schiestel, R., 2005. A new partially integrated transport model for subgrid-scale stresses and dissipation rate for turbulent developing flows. *Physics of Fluids* 17 (065106).
- Davidson, L., 2016. Zonal PANS: evaluation of different treatments of the RANS-LES interface. *Journal of Turbulence* 17 (3), 274–307.
- Davidson, L., 2019. Non-zonal detached eddy simulation coupled with a steady RANS solver in the wall region. *ERCOTAC Bulletin* 89, Special Issue on Current trends in RANS-based scale-resolving simulation methods.
- Davidson, Lars, Friess, Christophe, 2019. A new formulation of f_k for the PANS model. *Journal of Turbulence* 20 (5), 322–336.
- Davidson, Lars, Peng, Shia-Hui, 2003. Hybrid LES-RANS: A one-equation SGS model combined with a $k-\omega$ for predicting recirculating flows. *International Journal for Numerical Methods in Fluids* 43 (9), 1003–1018.
- Davidson, L., Friess, C., 2018. The PANS and PITM model: a new formulation of f_k . In: *Proceedings of 12th International ERCOTAC Symposium on Engineering Turbulence Modelling and Measurements (ETMM12)*, Montpellier, i France 26–28 September, 2018.
- Emvin, P., 1997. The Full Multigrid Method Applied to Turbulent Flow in Ventilated Enclosures Using Structured and Unstructured Grids. In: *Dept. of Thermo and Fluid Dynamics*. Chalmers University of Technology, Göteborg.
- Fadai-Ghotbi, Atabak, Friess, Christophe, Manceau, Rémi, Borée, Jacques, 2010. A seamless hybrid rans-les model based on transport equations for the subgrid stresses and elliptic blending. *Physics of Fluids* 22 (5), 055104 .
- Friess, Ch., Manceau, R., Gatski, T.B., 2015. Toward an equivalence criterion for hybrid RANS/LES methods. *Computers & Fluids* 122, 233–246.
- Girimaji, S.S., 2006. Partially-averaged Navier–Stokes model for turbulence: A Reynolds-averaged Navier–Stokes to direct numerical simulation bridging method. *ASME Journal of Applied Mechanics* 73 (2), 413–421.
- Greenblatt, D., Paschal, K.B., Yao, C.-S., Harris, J., Schaeffer, N.W., Washburn, A.E., 2004. A separation control CFD validation test case. Part 1: Baseline & steady suction. *AIAA-2004-2220*.
- Greenblatt, D., Paschal, K.B., Yao, C.-S., Harris, J., 2005. A separation control CFD validation test case Part 1: Zero efflux oscillatory blowing. *AIAA-2005-0485*.
- Gritskevich, M., Garbaruk, A., Schütze, J., Menter, F.R., 2012. Development of DDES and IDDES formulations for the $k-\omega$ shear stress transport model. *Flow, Turbulence and Combustion* 88, 431–449.
- Irannezhad, M., 2006. DNS of channel flow with finite difference method on a staggered grid. Msc thesis, Division of Fluid Dynamics, Department of Applied Mechanics, Chalmers University of Technology, Göteborg, Sweden.
- Klapwijk, M., Lloyd, T., Vaz, G., 2019. On the accuracy of partially averaged navier–stokes resolution estimates. *International Journal of Heat and Fluid Flow* 80, 108484 .
- Lee, M., Moser, R.D., 2015. Direct numerical simulation of turbulent channel flow up to $Re_\tau \approx 5200$. *Journal of Fluid Mechanics* 774, 395–415.
- Ma, J., Peng, S.-H., Davidson, L., Wang, F., 2011. A low Reynolds number variant of Partially-Averaged Navier–Stokes model for turbulence. *International Journal of Heat and Fluid Flow* 32 (3), 652–669.
- Orlandi, P., 2000. *Fluid Flow Phenomena – A Numerical Toolkit*. Kluwer Academic Publishers.
- Schiestel, Roland, Dejoan, Anne, 2005. Towards a new partially integrated transport model for coarse grid and unsteady turbulent flow simulations. *Theoretical and Computational Fluid Dynamics* 18 (6), 443–468.
- Shur, M.L., Spalart, P.R., Strelets, M.Kh., Travin, A.K., 2008. A hybrid RANS-LES approach with delayed-DES and wall-modelled LES capabilities. *International Journal of Heat and Fluid Flow* 29, 1638–1649.
- Spalart, P.R., Jou, W.-H., Strelets, M., Allmaras, S.R., 1997. Comments on the feasibility of LES for wings and on a hybrid RANS/LES approach. In: Liu, C., Liu, Z., (Eds.), *Advances in LES/DNS*, First Int. Conf. on DNS/LES, Louisiana Tech University. Greyden Press.
- Spalart, P., Deck, S., Shur, M., Squires, K., Strelets, M., Travin, A., 2006. A new version of detached-eddy simulation, resistant to ambiguous grid densities. *Theoretical and Computational Fluid Dynamics* 20, 181–195. <https://doi.org/10.1007/s00162-006-0015-0>.
- Wallin, S., Johansson, A.V., 2000. A new explicit algebraic Reynolds stress model for incompressible and compressible turbulent flows. *Journal of Fluid Mechanics* 403, 89–132.